PHILOSOPHICAL TRANSACTIONS OF THE ROYAL SOCIETY B BIOLOGICAL SCIENCES

# Probabilistic Secretion of Quanta in the Central Nervous System: Granule Cell Synaptic Control of Pattern Separation and Activity Regulation

W. G. Gibson, J. Robinson and M. R. Bennett

*Phil. Trans. R. Soc. Lond. B* 1991 **332**, 199-220
doi: 10.1098/rstb.1991.0050

# Probabilistic secretion of quanta in the central nervous system: granule cell synaptic control of pattern separation and activity regulation

W. G. GIBSON, J. ROBINSON AND M. R. BENNETT†

*Department of Applied Mathematics, Department of Mathematical Statistics and Neurobiology Research Centre, University of Sydney, New South Wales 2006, Australia*

## CONTENTS

1. Introduction 200
2. Model network 200
   (*a*) Output in the absence of an inhibitory interneuron 202
   (*b*) Output with a linear inhibitory interneuron 203
3. Stochastic secretion of quanta at granule cell synapses 204
   (*a*) Stochastic secretion: temporal variability in transmitter secretion 204
   (*b*) Stochastic secretion: spatial variability in transmitter secretion 205
4. Stochastic secretion and the regulation of granule-cell output activity 205
   (*a*) Output in the absence of an inhibitory interneuron 207
   (*b*) Output with a linear inhibitory interneuron 207
   (*c*) Output with a nonlinear inhibitory interneuron 207
5. Stochastic secretion and the separation of patterns 209
   (*a*) The effect of spatial variability in transmitter secretion 209
   (*b*) The effect of temporal variability in transmitter secretion 210
6. Analytic approximations 211
   (*a*) An analytic approximation for the output activity of granule cells 211
   (*b*) An analytic approximation for pattern separation by granule cells 212
7. Conclusion: physiological studies of the model network and the role of probabilistic secretion of quanta 212
   (*a*) The cerebellar granule-cell/Golgi-cell neural network 212
   (*b*) The hippocampal granule-cell/basket-cell neural network 213
   (*c*) Experimental testing of the model networks and the role of probabilistic secretion of quanta 214
   (*d*) Output control and memory storage 215
8. Appendix
   (*a*) Analytic expressions for granule-cell output and pattern separation in various cases 215
   (*b*) The relation between spatial and temporal variability of synapses and probabilistic firing of neurons 216
   (*c*) Nonlinear model for the inhibitory interneuron 217
   (*d*) Analytic approximations for granule-cell output and pattern separation 217
   (*e*) Simulation methods 218

References 219

## SUMMARY

The implications of probabilistic secretion of quanta for the functioning of neural networks in the central nervous system have been explored. A model of stochastic secretion at synapses in simple networks, consisting of large numbers of granule cells and a relatively small number of inhibitory interneurons, has been analysed. Such networks occur in the input to the cerebellum Purkinje cells as well as to hippocampal CA3 pyramidal cells and to pyramidal cells in the visual cortex. In this model the input axons terminate on granule cells as well as on an inhibitory interneuron that projects to the granule cells. Stochastic secretion at these synapses involves both temporal variability in secretion at single synapses in the network as well as spatial variability in the secretion at different synapases. The role of this stochastic

† To whom correspondence should be addressed: Neurobiology Research Centre, University of Sydney.

variability in controlling the size of the granule cell output to a level independent of the size of the input and in separating overlapping inputs has been determined analytically as well as by simulation.

The regulation of granule-cell output activity to a reasonably constant value for different size inputs does not occur in the absence of an inhibitory interneuron when both spatial and temporal stochastic variability occurs at the remaining synapses; it is still very poor in the presence of such an interneuron but in the absence of stochastic variability. However, quite good regulation is achieved when the inhibitory interneuron is present with spatial and temporal stochastic variability of secretion at synapses in the network. Excellent regulation is achieved if, in addition, allowance is made for the nonlinear behaviour of the input–output characteristics of inhibitory interneurons.

The capacity of granule-cell networks to separate overlapping patterns of activity on their inputs is adequate, with spatial variability in the secretion at synapses, but is improved if there is also temporal variability in the stochastic secretion at individual synapses, although this is at the expense of reliability in the network. Other factors which improve pattern separation are control of the output to very low activity levels, and a restriction on the cumulative size of the excitatory input terminals of each granule cell.

Application of the theory to the input neural networks of the cerebellum and the hippocampus shows the role of stochastic variability in quantal transmission in determining the capacity of these networks for pattern separation and activity regulation.

## 1. INTRODUCTION

An important source of natural variability in any neural network is the probabilistic secretion of transmitter quanta at synapses (Katz 1969; Bennett *et al.* 1977; Redman & Walmsley 1982; Korn & Faber 1987). The statistics of secretion at single synapses has been analysed in detail (Bennett & Robinson 1990; Redman 1990) but its implications for the functioning of neural networks has not been much explored (Little & Shaw 1975; Burnod & Korn 1989). In the present work we have examined the effects of probabilistic quantal secretion at synapses in realistic neural networks of granule cells and inhibitory interneurons.

Granule cells exist in very large numbers, compared with other neuron types, at the input to the cerebellum, hippocampus and visual cortex (Cajal 1911; Lorente de Nó 1933, 1934). Marr (1969, 1970) suggested that these granule cells might serve at least two functions: one of these is to orthogonalize overlapping inputs; the other, in conjunction with inhibitory interneurons, is to ensure that large inputs do not saturate the system, by restricting them to a relatively constant size. The granule cells then perform the function of pattern-separation and the inhibitory interneurons perform the additional function of ensuring that the number of active fibres is kept within acceptable bounds by controlling the threshold of the granule cells (Willis 1975, 1986).

Only the granule cell networks of the cerebellum have been analysed in detail (Marr 1969; Albus 1971; Torioka 1978), although roles for the granule cells in the fascia dentata of the hippocampus have been indicated (Marr 1971; McNaughton & Morris 1987; McNaughton & Nadel 1989). Torioka (1979), by using a two-layered neural network with inhibitory connections that utilized threshold elements, showed the importance of inhibitory connections in the cerebellum for pattern separation and how the standard deviation of the threshold values of the threshold elements also contributed to pattern separation; maintaining this standard deviation to a small-value greatly enhanced pattern-separation (Torioka & Ikeda 1988).

This work presents analytical solutions and Monte Carlo simulations of the functioning of the granule cell network in the cerebellum and the hippocampus. It shows that pattern separation and the control of the size of the output to a level independent of the size of the input are both greatly improved by the stochastic nature of quantal secretion at synapses. The paper is organized as follows. In §2 the model network is described and basic quantities such as activity level and pattern overlap are defined. Then the behaviour of the network is studied in the absence of any stochastic secretion of transmitter at synapses. This work serves to show the formalism in a simple context, and to emphasize the severe limitations of the model if stochastic secretion is not included. In §3 the nature of stochastic secretion of quanta at granule-cell synapses is described, with emphasis on the fact that the total variability contains both a spatial and a temporal aspect. §§4 and 5 then incorporate this synaptic variability into the basic model network, first without an inhibitory interneuron, then with a linear one and finally with a more biologically plausible nonlinear one. §6 is concerned with the development and application of analytic approximations which work well in precisely the case where computer simulation of the network becomes difficult, namely when the granule cells have many excitatory inputs, as is the case for the hippocampus. §7 provides the conclusion by first showing the relevance of the model network to the functioning of the input to the cerebellum and the hippocampus; it then provides an experimental procedure for testing the suggested function of these networks and the role of probabilistic secretion of quanta.

## 2. MODEL NETWORK

The basic model neural network is the two-layer system shown in figure 1*a*. The input layer consists of $n$ neurons, and the output contains $N$ neurons (granule cells). It is assumed that each granule cell receives




PHILOSOPHICAL TRANSACTIONS OF THE ROYAL SOCIETY B BIOLOGICAL SCIENCES

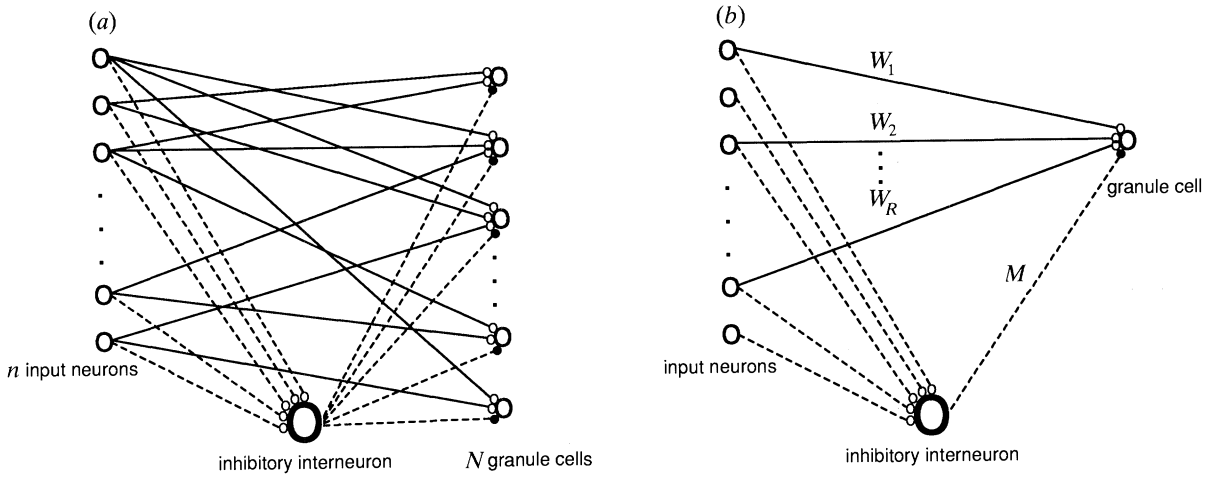


Figure 1. (*a*) Structure surrounding one inhibitory interneuron (IIN). The $n$ input neurons form direct excitatory connections with the $N$ granule cells, with $R$ input fibres synapsing with each granule cell. The connections are random, in the sense that each of the $R$ inputs has probability $1/n$ of coming from a given input fibre. Each input fibre thus branches an average of $NR/n$ times. All the input neurons form excitatory synapses with the IIN, which in turn forms inhibitory connections with each granule cell. Typical values are $60 < n < 100$, $N \approx 5700$, $R \approx 4$ in the case of the cerebellum. (*b*) Structure around one granule cell. The typical granule cell has $R$ inputs, chosen at random from the $n$ input fibres. These are relabelled $1, 2, \ldots, R$, and the connections weighted by random variables $W_1, W_2, \ldots, W_R$, which represent the amount of transmitter released when the input fibre is active. $M$ is the corresponding weight for the IIN-to-granule cell connection.

exactly $R$ inputs, from $R$ different input neurons. The connections are taken to be random, in the sense that each of the granule-cell inputs has probability $1/n$ of coming from a given input neuron. All $n$ input neurons also make excitatory connections with the inhibitory interneuron (IIN), which in turn makes inhibitory connections with all the $N$ granule cells.

In the following, it is the statistical properties of the system that are to be studied: for example, the average output on the granule cells when a large number of different patterns are placed on the input neurons. Therefore the precise behaviour of individual granule cells under completely specified inputs is not required. The desired quantities can be obtained by considering one typical granule cell, and then averaging over a distribution of synaptic weights. More precisely, a randomly selected granule cell is considered. This makes synaptic connections with $R$ input neurons chosen randomly from the $n$ available. These $R$ neurons are renumbered $1, 2, \ldots, R$, and the stochastic nature of synaptic transmission is accounted for by assuming that the amounts of transmitter secreted at the corresponding synaptic terminals are random variables $W_1, W_2, \ldots, W_R$. (See figure 1*b* and §8*e*). The $W_k$'s take into account both the variability in a single terminal, which is of a temporal nature, and the spatial variability between terminals. The temporal variability results in differing secretions from a single terminal; the spatial variability includes variation among the $R$ terminals on one granule cell and between different granule cells. There will also be variability in transmission from the input neurons to the IIN, but because the IIN sums a large number of potentials it is not necessary to assign different weights to these inputs (see §4*c*). The single connection from the IIN to the granule cell is assigned a weight $M$, which is again a random variable incorporating both spatial and temporal variability. This stochastic variability will be treated in detail in §3; for the rest of this section all weights will be taken to be fixed.

Consider now the network shown in figure 1*b*. A pattern on the input neurons is given by the vector $\boldsymbol{x} = (x_1, x_2, \ldots, x_n)$, where $x_i$ is 1 if the $i$th input neuron is active and is 0 otherwise. Since the granule cell is chosen at random, the order of elements in $\boldsymbol{x}$ may be ignored and it can be assumed that $x_1, x_2, \ldots, x_n$ are independent random variables with

$$\phi = P(x_i = 1), \quad i = 1, 2, \ldots, n. \tag{1}$$

That is, $\phi$ is the probability that a randomly selected input is active; it will be called the activity level for pattern $\boldsymbol{x}$. Because $x_i$ takes values 1, 0 only, then $E(x_i) = \phi$, where $E$ denotes the average or expectation of a random variable. The granule cells are assumed to perform a linear summation on their inputs; that is, the synaptic potentials due to different active input fibres add linearly, no account being taken of nonlinear summation problems (McLachlan & Martin 1981). Thus the total input of transmitter to the typical granule cell from the input neurons is

$$Q = \sum_{k=1}^{R} W_k x_k. \tag{2}$$

The granule cells are taken to be threshold units, and thus fire if $Q > H(\phi)$, where $H(\phi)$ is the total threshold on the granule cell. It is given by

$$H(\phi) = \theta_0 + \theta(\phi), \tag{3}$$

where $\theta_0$ is the intrinsic threshold on the granule cell and $\theta(\phi)$, which will be positive, is the contribution arising from the IIN. If the granule cell performs a linear summation on the IIN output, then

$$\theta(\phi) = MG(\phi), \tag{4}$$




PHILOSOPHICAL TRANSACTIONS OF THE ROYAL SOCIETY B BIOLOGICAL SCIENCES

where $G(\phi)$ is the total IIN output, and $M$ is the synaptic weight described above. This is probably a good first approximation but the actual dependence of $\theta(\phi)$ on $G(\phi)$ is likely to be more complicated. A more realistic model is described in §4*c*.

The output pattern on the set of $N$ granule cells is denoted by $\boldsymbol{X} = (X_1, X_2, \ldots, X_N)$ where $X_i$ is 0 or 1. The output activity level is

$$\Phi = P(X_i = 1), \quad i = 1, 2, \ldots, N, \tag{5}$$

where again, under the statistical assumptions, the activity level is independent of the particular granule cell considered. It follows that $\Phi = E(X_i)$; also

$$\Phi = P(Q > H), \tag{6}$$

that is, the output activity level $\Phi$ is given by the probability that the input $Q$ to the granule cell exceeds its threshold $H$.

The activities $\phi$ and $\Phi$ may be thought of as averages in the following sense: for a large system containing many input fibres and granule cells, $\phi$ is the fraction of input fibres active when pattern $x$ is presented, and $\Phi$ is the fraction of granule cells activated as a result. Equivalently, suppose a number of different input patterns are placed sequentially on the input fibres, with all patterns having the same average fraction $\phi$ of fibres active, but with the sequence of active and inactive fibres entirely random. If the number of patterns presented is large, then one can focus attention on just one (randomly chosen) input fibre: $\phi$ will be the fraction of times that this input fibre is active. Also, in the case where all the weights $W_k$ and $M$ are fixed and equal, it is only necessary to look at one (also randomly chosen) granule cell: $\Phi$ will be the fraction of times this granule cell fires. In the case where the weights are variable it is necessary to sample the output from a number of granule cells; however, even here one can consider the (mathematically) equivalent situation of looking at just one granule cell, but treating the weights as random variables. This is the approach taken when doing computer simulations of the network, and further details are given in §8*e*.

To investigate pattern separation it is necessary to consider two input patterns, $\boldsymbol{x}$ and $\boldsymbol{y}$, as well as their corresponding outputs $\boldsymbol{X}$ and $\boldsymbol{Y}$, to find the overlaps when the input patterns are placed sequentially on the input neurons. There are now two input activity levels $\phi_x$ and $\phi_y$, and also an input overlap activity

$$\psi_{xy} = P(x_i y_i = 1), \quad i = 1, 2, \ldots, n. \tag{7}$$

Thus $\psi_{xy}$ is the probability that an input neuron is active under both pattern $\boldsymbol{x}$ and pattern $\boldsymbol{y}$. The actual overlap is measured by the quantity

$$\tau_{xy} = \psi_{xy} / \sqrt{(\phi_x \phi_y)}. \tag{8}$$

For $n$ large, $\tau_{xy}$ can be interpreted as the cosine of the angle between $\boldsymbol{x}$ and $\boldsymbol{y}$, where the patterns are considered as vectors in an $n$-dimensional space.

The output overlap is measured by

$$T_{xy} = \Psi_{xy} / \sqrt{(\Phi_x \Phi_y)}, \tag{9}$$

where $\Phi_x$ and $\Phi_y$ are the output activities for $\boldsymbol{X}$ and $\boldsymbol{Y}$ respectively, and the overlap probability $\Psi_{xy}$ is defined by an equation analogous to (7). Again, $T_{xy}$ has an interpretation as the cosine of an angle. Thus the line $T_{xy} = \tau_{xy}$ corresponds to no improvement in pattern separation and the region below this line represents an improvement.

One can also consider the situation in which many pattern pairs $\{\boldsymbol{x}, \boldsymbol{y}\}$ are presented to the network; $\tau_{xy}$ is then related to the fraction of times that a randomly chosen input fibre is active under both patterns in a pair, and $T_{xy}$ is related to the fraction of times that a randomly chosen granule cell is fired by both members of a pair. (For the precise relations, one must use (8) and (9).) Again, in the variable-weight case, sampling from different granule cells is equivalent to monitoring the output of a single granule cell, but with the weights applied as random variables. §8*e* gives details as to how this approach is used in computer simulation.

It is to be emphasized that it is not the actual ordering of 1's and 0's in an input or output pattern that is of interest in this work. Rather, it is the activity levels $\phi$ and $\Phi$, to which are now added the quantities $\psi$, $\Psi$, $\tau$ and $T$ characterizing pattern overlap. In this way it is possible to analyse the behaviour of a network with an arbitrary (large) number of input and output neurons (figure 1*a*) by averaging over the behaviour of a subsystem (figure 1*b*).

Let $H_x$, $H_y$ be the granule cell thresholds for inputs $\boldsymbol{x}, \boldsymbol{y}$, respectively. From (3), $H_x = \theta_0 + \theta(\phi_x)$, $H_y = \theta_0 + \theta(\phi_y)$ and the output activities can be expressed as $\Phi_x = P(Q_x > H_x)$, $\Phi_y = P(Q_y > H_y)$ and

$$\Psi_{xy} = P[(Q_x > H_x) \cap (Q_y > H_y)]. \tag{10}$$

### (*a*) *Output in the absence of an inhibitory interneuron*

First consider the situation which would prevail if the IIN were absent. In this case, the total threshold on the granule cell is just the intrinsic threshold: $H = \theta_0$. If all the weights $W_k$ are equal (and without loss of generality they can be taken to be unity), the output activity is simply a sum of binomial probabilities (§8*a*(i)):

$$\Phi = \sum_{k > \theta_0}^{R} b(k; R, \phi). \tag{11}$$

Figure 2*a* shows the output activity $\Phi$ plotted against the input activity $\phi$ for $R = 4$ and four different choices of $\theta_0$. Note that it makes no difference which particular value of $\theta_0$ is chosen in each interval, since for $W_k = 1$ the total input to a granule cell is an integer.

The output control shown here is very poor: a low threshold gives almost no control, with $\Phi$ rapidly becoming large; a high threshold severely restricts the output for small $\phi$, but again is ineffectual for large $\phi$. These extremes are undesirable: a very small output means that information encoded in the input patterns will be lost; a large output will lead to overload in subsequent stages of the network. (This has been discussed in the context of the cerebellum by Marr (1969) and Albus (1971).) Figure 2*a* shows that there




PHILOSOPHICAL TRANSACTIONS OF THE ROYAL SOCIETY B BIOLOGICAL SCIENCES

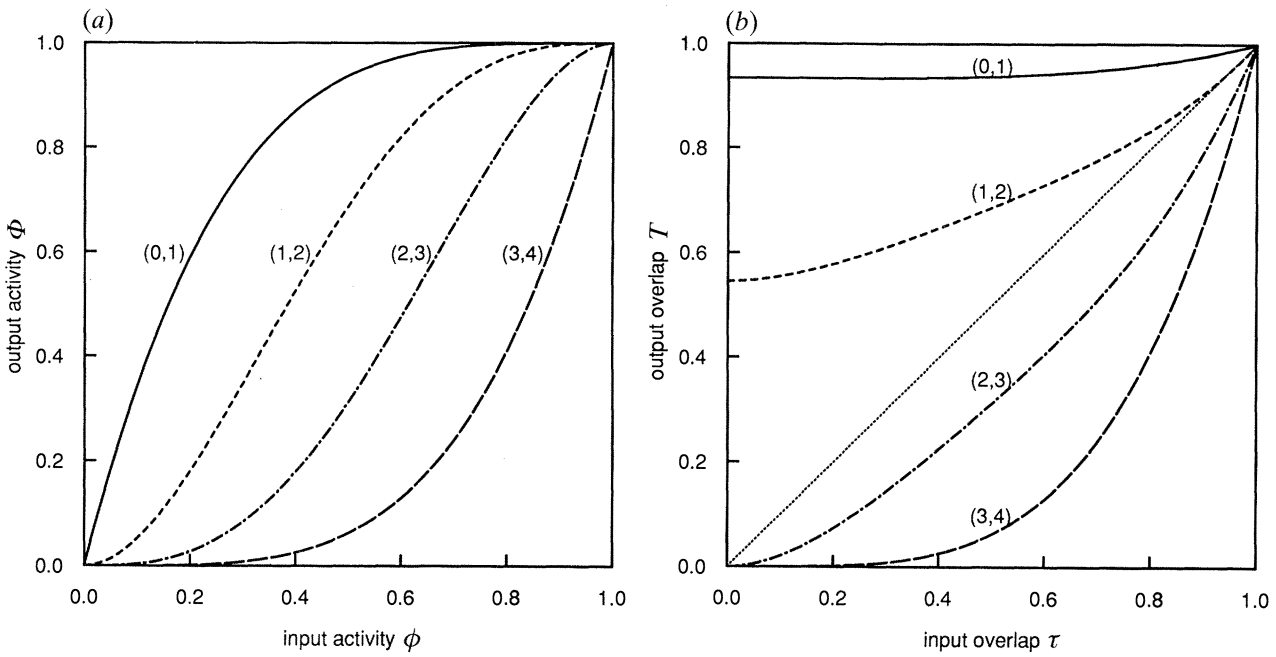


Figure 2. (*a*) Granule-cell output in the absence of an IIN and with fixed weights. The output activity level $\Phi$ on the granule cells is plotted against the input activity level $\phi$ on the input fibres. All connections have unit weight and the number of input fibres connecting to each granule cell is $R = 4$. The four curves are, from left to right, for the intrinsic granule cell threshold $\theta_0$ in the ranges $(0, 1)$, $(1, 2)$, $(2, 3)$ and $(3, 4)$, respectively. The exact value of $\theta_0$ in each of these ranges does not matter, since the total input to the granule cell can take only integer values. (*b*) Pattern separation in the absence of an IIN and with fixed weights. The output overlap $T_{xy}$ is plotted as a function of the input overlap $\tau_{xy}$. The graph is drawn for the same four cases as in (*a*), with input activities $\phi_x = \phi_y = 0.5$. Pattern separation is very good for the $(3, 4)$, but since this model does not control $\Phi$ this is not of any significance.

is only a small range of $\phi$ values for which the output is of a reasonable magnitude.

Pattern separation is given by

$$\Psi_{xy} = \sum_{p>\theta_0}^{R} \sum_{q>\theta_0}^{R} W_{pq}, \tag{12}$$

where $W_{pq}$ is a sum over multinomial distributions (§8*a*(i)). $T_{xy}$ can then be calculated as a function of $\tau_{xy}$ by using (8) and (9). Figure 2*b* shows this relation for the case $R = 4$, $\phi_x = \phi_y = 0.5$ and the four values of $\theta_0$ used in figure 2*a*. Pattern separation is very good for the case $3 < \theta_0 < 4$, but since this model fails to regulate $\Phi$ this result is not really of any significance.

It is instructive to relate the early work of Marr (1969) on pattern separation in the cerebellum to the present treatment. Marr did not take account of variability in synaptic transmission ($W_k = 1$), and initially assumed that all $R$ inputs had to be active before a granule cell would fire. This corresponds to setting $R-1 < \theta_0 < R$ in the present treatment, so $\Phi = \phi^R$ and $\Psi_{xy} = (\psi_{xy})^R$, leading to $T_{xy} = (\tau_{xy})^R$. For the case $R = 4$, this corresponds to the lowest curves in figure 2*a*, *b*. Thus separation is optimal but, as pointed out above, $\Phi$ is so poorly controlled that such a system works for only a very restricted range of $\phi$ values. Marr subsequently relaxes the above threshold condition (with the introduction of variable codon size), but the output control remains relatively crude.

### (*b*) *Output with a linear inhibitory interneuron*

The previous section shows that some mechanism, over and above a fixed threshold on the granule cells, is necessary for the regulation of the level of output activity on the granule cells. Marr (1969) suggested that the IIN plays an important role in this regard, and this will now be investigated, using a simple linear model; a more complex and physiologically realistic one will be given in §4*c*.

About the simplest assumption one can make is that the IIN output is directly proportional to its input so that its action is essentially just that of a summing device. If no account is taken of any variability in the effect of each input neuron input to the IIN, then the average total input is simply proportional to the activity level $\phi$ of the input neurons. Thus the output of the IIN is taken to be $G(\phi) = c\phi$, where c is a constant, and the total threshold on a granule cell becomes $H(\phi) = \theta_0 + c\phi$. If there is also no variability in the input neuron to granule cell connections (i.e. all $W_k = 1$), then the theory of §8*a*(i) applies and $\Phi$ is given by (11), with $\theta_0$ replaced by $H$. This leads to the characteristic 'saw-tooth' shape shown by the solid line in figure 3*a*, where $\Phi$ is plotted as a function of $\phi$ for the case $R = 4$, $H = 1 + 4\phi$. The 'jumps' occur at those values of $\phi$ for which $H(\phi)$ takes integer values 1–4, since for $W_k = 1$ the total input to a granule cell is integral, and so as $H(\phi)$ increases through an integral value the granule cell requires an additional active input before it fires. It is clear that this general behaviour is not dependent on the detailed output

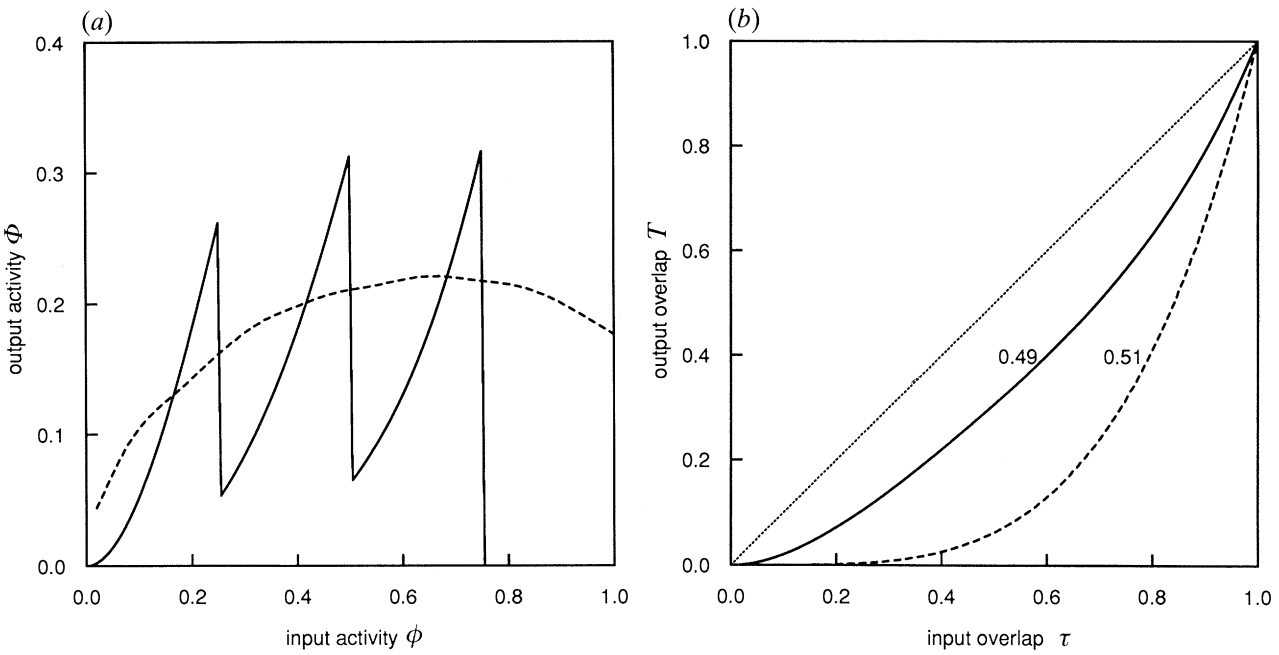


Figure 3. (*a*) Granule cell output for the linear IIN model. The output activity $\Phi$ is plotted against the input activity $\phi$ for a network incorporating the linear IIN model. In this model the total threshold on a granule cell is $H = \theta_0 + c\phi M$, where $\theta_0$ is the intrinsic threshold of the granule cell, $c\phi$ is the contribution from the IIN, taken to be simply proportional to its total input, and $M$ is the weight on the IIN-to-granule cell connection. For this graph, $R = 4$ and $H = 1 + 4\phi M$. (——), Weights $W_k$ and $M$ are fixed at 1.0. The 'jumps' occur at those values of $\phi$ at which $H$ takes integer values, i.e. at $\phi = 0.25, 0.5, 0.75$. At each of these values an extra input must become active to fire the granule cell. Thus output control is very poor, and the model has the highly undesirable feature that a very small change in input activity can drastically alter the output activity. (------), Weights $W_k$ and $M$ are normal random variables, with means 1.0 and standard deviations $\sigma_W = 0.5$ and $\sigma_M = 0.1$, respectively. Calculation is by simulation (appendix 7.5). The effect of stochastic variation in $W_k$ and $M$ has been to remove the 'jumps', and give $\Phi$ a smooth dependence on $\phi$. (*b*) Pattern separation for the linear IIN model with fixed weights $W_k = 1$ and $M = 1$. The output overlap $T_{xy}$ is plotted as a function of the input overlap $\tau_{xy}$ for a network with the same parameters as for the solid curve of (*a*). (——), $\phi_x = \phi_y = 0.49$; (------), $\phi_x = \phi_y = 0.51$. Although these input activities are close, they are on opposite sides of a large jump in output activities (see (*a*) of this figure) and hence lead to very different pattern separations.

from the IIN, any reasonable output will lead to a sawtooth graph. It would require a highly nonlinear IIN output, following exactly the peaks and troughs of figure 3*a*, to level the granule cell output.

The output overlap is given by (12), with the lower limits on the sums replaced by $H_x$ and $H_y$. Pattern separation depends crucially on the values of $H_x$ and $H_y$ and hence on $\phi_x$ and $\phi_y$. Figure 3*b* shows the output overlap $T_{xy}$ as a function of the input overlap $\tau_{xy}$ for the case where $R = 4$ and $H = 1 + 4\phi$. The solid curve is for $\phi_x = \phi_y = 0.49$: as can be seen from the solid curve in figure 3*a*, this value occurs just before a downwards jump and gives a relatively high output activity ($\Phi \approx 0.3$) which leads to poor pattern separation. The broken curve is for $\phi_x = \phi_y = 0.51$: this value occurs just after the jump and gives a low output activity ($\Phi \approx 0.07$) which leads to good separation. But it makes no physiological sense to have pattern separation so highly sensitive to small changes in the input; $\Phi$ should be at least a smooth function of $\phi$. Thus additional control mechanisms must be sought.

## 3. STOCHASTIC SECRETION OF QUANTA AT GRANULE CELL SYNAPSES

In the previous section it was shown that satisfactory control of the granule-cell output activity $\Phi$ cannot be achieved in a network with fixed synaptic weights; even the presence of an inhibitory interneuron does not give anything like constant output. The next step is to take into account the variability in the strengths of the connections between various neurons. This variability occurs because of the stochastic nature of quantal release at synaptic terminals, and as mentioned previously has both a temporal and a spatial aspect. This is now considered in more detail.

### (*a*) *Stochastic secretion: temporal variability in transmitter secretion*

Consider a single synaptic terminal, and suppose that it has $\nu$ release sites. In the general case, these sites will have different probabilities $p_1, p_2, \ldots, p_\nu$ of releasing a single quantum of transmitter when active. In the particular case where all these probabilities are equal to $p$ the total number $X$ of quanta released at the terminal follows a binomial distribution with parameters $\nu$ and $p$:

$$P(X = r) = b(r; \nu, p) \equiv \binom{\nu}{r} p^r (1-p)^{\nu - r}. \qquad (13)$$

The quantal size $Z$ is not fixed, but follows a unimodal distribution which will be assumed to be normal with

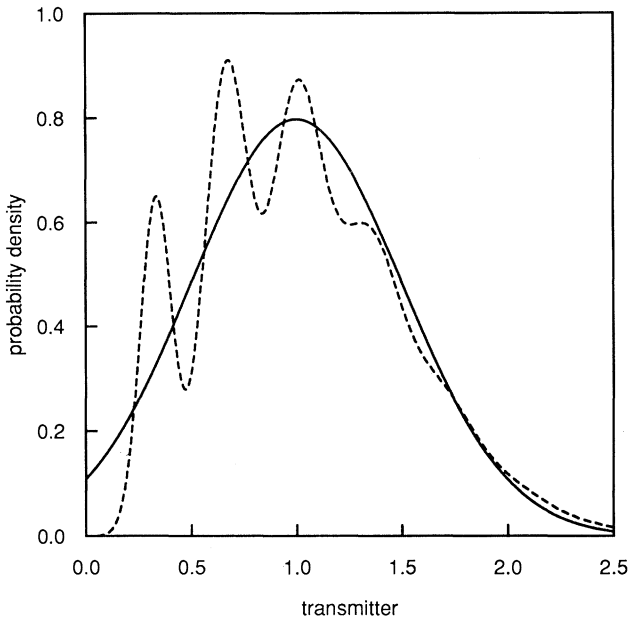


Figure 4. Probability density function for transmitter release at a single terminal. The terminal contains $\nu$ release sites, each of which releases a quantum of transmitter with a certain probability $p_i, i = 1, 2, \ldots, \nu$, when active. The quantal size is taken to be normally distributed, and the broken curve gives the distribution of the total amount of transmitter, $W$ (equation (14)), for the case where all the probabilities are equal ($p_i = p, i = 1, 2, \ldots, \nu$). The solid curve is the normal distribution $N(m, s^2)$. (Actual value used in drawing the curves are $\nu = 10$, $p = 0.3$, $\mu = 0.333$, $\sigma = 0.075$, giving $m = 1$, $s = 0.5$.) In subsequent calculations the normal curve will be used. In every application much averaging occurs and hence the fact the normal curve is a smoothed version of the more accurate distribution is of no consequence.

mean $\mu$ and variance $\sigma^2$. Since the quanta are to be added, this assumption is not of crucial importance, and any similar distribution would be acceptable. The total amount $W$ of transmitter released at the whole terminal is thus a sum of $X$ independent, identically distributed random variables $Z$: $W = Z_1 + Z_2 + \ldots + Z_X$. It follows that $W$ has mean $m = \nu\bar{p}\mu$ and variance $s^2 = \nu[\bar{p}(1-\bar{p}) - \sigma_p^2]\mu^2 + \nu\bar{p}\sigma^2$, where $\bar{p} = \sum_{i=1}^{\nu} p_i/\nu$ and $\sigma_p^2 = \sum_{i=1}^{\nu} (p_i - \bar{p})^2/\nu$. Thus $W$ has density function

$$f_W(w) = \sum_{r=1}^{\nu} \frac{1}{\sigma\sqrt{(2\pi r)}} \exp\left(-\frac{(w-r\mu)^2}{2r\sigma^2}\right) b(r; \nu, \boldsymbol{p}). \quad (14)$$

(cf. Robinson 1976). $W$ may be looked upon as the weight associated with a single connection from input neuron to granule cell.

In the calculations performed in this work the distribution (14) has, for simplicity, been replaced by a normal distribution with mean $m$ and variance $s^2$ as given above. The relation of this normal distribution to (14) is shown in figure 4, where the broken curve comes from (14) and the solid curve is the normal density function with parameters $m$ and $s^2$. The normal curve gives a smoothed version but, because of further averaging, both spatial and temporal, this difference is of no consequence and produces effectively the same results.

### (*b*) *Stochastic secretion: spatial variability in transmitter secretion*

The parameters $\nu, p_1, p_2, \ldots, p_\nu, \mu, \sigma$ and hence $m, s^2$, introduced in the previous section are fixed for a given terminal, but vary from terminal to terminal, both on the same and on different granule cells. In other words, they are conditional on the terminal chosen, and if the weights are now labelled $W_k$, where $k$ is the terminal number, then $m$ and $s^2$ should be replaced by $m_k = E(W_k|k)$ and $s_k^2 = \mathrm{var}(W_k|k)$. Thus $m_k$ is a random variable; for a given value of $k$ it is the time-averaged amount of transmitter released at the $k$th terminal when it is active. If $m_k$ has mean $\mu_W$ and variance $\sigma_S^2$, then the overall mean of $W_k$, including both spatial and temporal variability, is $\mu_W$ and the overall variance is $\sigma_S^2 + \sigma_T^2$, where $\sigma_T^2 = E(s_k^2)$.

Each input neuron-to-granule cell weight $W_k$ can thus be written as the sum of two random variables,

$$W_k = W_k^S + W_k^T, \quad (15)$$

where $W_k^S \equiv m_k$ is the *spatial* part and $W_k^T \equiv W_k - m_k$ is the *temporal* part. Thus $W_k^S$ varies only with $k$; for fixed $k$, corresponding to repeated inputs on the same terminal, it is a constant. On the other hand, $W_k^T$ changes from input to input, even for fixed $k$; that is, the same terminal. Thus $W_k^S$ may be looked upon as a measure of the number of release sites which a terminal possesses, whereas $W_k^T$ is a measure of the temporal fluctuations which occur around a mean value. As explained above, both $W_k^S$ and $W_k^T$ will be taken to be normal random variables, with distributions $N(\mu_W, \sigma_S^2)$ and $N(0, \sigma_T^2)$, respectively, so that

$$\sigma_W^2 = \sigma_S^2 + \sigma_T^2. \quad (16)$$

This distinction between spatial and temporal variation is not relevant to the consideration of the control function of the network, since this involves looking at the results of a single input (§4), but it is of importance for pattern separation, which involves two separate inputs (§5).

There is an alternative treatment of synaptic transmission, in which only the spatial variation is included in the weights, and the temporal variation is taken into account by introducing a certain probability function which governs the firing of the neuron. Its relation to the present formalism is given in §8*b*.

## 4. STOCHASTIC SECRETION AND THE REGULATION OF GRANULE-CELL OUTPUT ACTIVITY

The effect of stochastic secretion of transmitter, considered in §3, will now be incorporated into the model network of §2, first without an inhibitory interneuron, then with a simple linear one, and finally with a more realistic nonlinear one. Only output control is considered in this section, so there is no need to separate stochastic secretion into its spatial and temporal components: only the total variability is




PHILOSOPHICAL TRANSACTIONS OF THE ROYAL SOCIETY B BIOLOGICAL SCIENCES

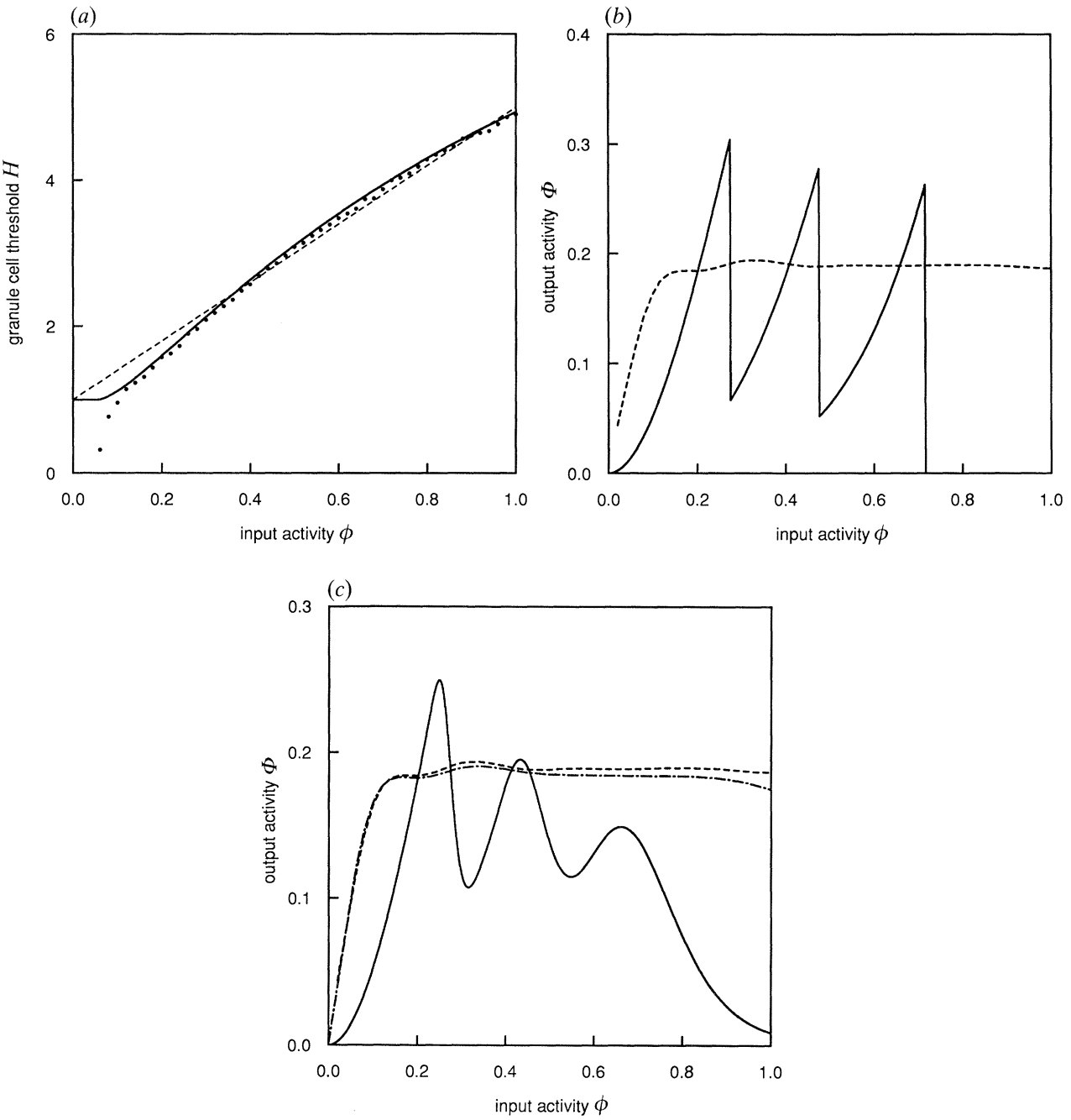


Figure 5. (*a*) Granule cell threshold for $\Phi = 0.2$. The total granule cell threshold $H$ is plotted as a function of the input fibre activity $\phi$. The points are the result of a computer simulation of the actual threshold needed to control the output to $\Phi = 0.2$. Parameters used are $R = 4$, $\mu_W = \mu_M = 1.0$, $\sigma_W = 0.5$, $\sigma_M = 0.1$. (——), Nonlinear model; (------), linear model: $H = 1.0 + 4\phi$. The solid curve is the result of fitting the general form $H = \theta_0 + c_1/\{1 + c_2/[(\phi/\phi_0) - 1.0 - \ln(\phi/\phi_0)]\}$, $\phi > \phi_0$. In such a fitting there is some flexibility in fixing the parameters, but this is not excessive; the values of $\theta_0$ and $\phi_0$ are to a large extent dictated by the behaviour of $H$ for small $\phi$. $\theta_0$ is the $\phi = 0$ limit of $H$, and can be taken as the value at which the linear approximation to $H$, shown by the broken line in (*a*), crosses the axis. The IIN does not fire at all for $\phi < \phi_0$ and so $H = \theta_0$ in this range; from (*a*) this restricts the choice to $0 \leqslant \phi_0 \lesssim 0.1$ and a value of 0.05 is reasonable. Once $\theta_0$ and $\phi_0$ are chosen, $c_1$ and $c_2$ are uniquely determined by fitting the curve at two additional points. (The points $\phi = 0.2$ and $\phi = 0.8$ were used in the present case, but the choice is not crucial, any two points in the range $0.15 < \phi < 1.0$ would give almost the same result.) The result of this procedure is $\theta_0 = 1.0$, $\phi_0 = 0.5$, $c_1 = 10.45$ and $c_2 = 26.5$, giving the threshold function $H = 1.0 + 10.45/\{1.0 + 26.5/[20\phi - 1.0 - \ln(20\phi)]\}$, $\phi > 0.05$. (*b*) Granule cell output for the nonlinear IIN model: comparison of fixed and variable weights. The threshold function is the nonlinear one shown as the solid line in (*a*). (——), All weights equal to unity. This shows very little improvement on the corresponding curve in figure 3*a*; indeed, it would require a very highly nonlinear IIN of an extremely specialized nature to achieve much smoothing in the absence of stochastic variation in transmitter release. (------), $W_k$ and $M$ normally distributed, with means 1 and standard deviations 0.5 and 0.1, respectively. (The calculation was performed with $M$ in its correct position as given by (18), but a repeat calculation with the approximation (19) showed that there was very little difference in this case.) This shows that very good output control can be achieved, over a wide range of input activity, by a combination of variable transmitter release and nonlinear behaviour in the IIN. Comparison with the broken curve




PHILOSOPHICAL TRANSACTIONS OF THE ROYAL SOCIETY B BIOLOGICAL SCIENCES

relevant since only one pattern ($\boldsymbol{x}$) is being presented. The distinction between spatial and temporal only becomes important for pattern separation, and this is treated in §5.

### (*a*) *Output in the absence of an inhibitory interneuron*

The effect of variable $W_k$ can be investigated, still under the assumption of no IIN. If $W_k$ is normally distributed, then the output activity $\Phi$ can be calculated exactly (§8*a*(iii)). The results of such calculations show that there is only a relatively minor change from the fixed-weight case shown in figure 2*a*. Thus a simple fixed threshold on the granule cells, even in the presence of stochastic transmitter secretion from the input fibres, cannot perform more than a rudimentary control on the output activity $\Phi$; in particular, it cannot even begin to control $\Phi$ to a constant level over a wide range of input activities.

### (*b*) *Output with a linear inhibitory interneuron*

The linear IIN described by $G(\phi) = c\phi$ is now included. From (3) and (4) the granule-cell threshold is $H = \theta_0 + Mc\phi$, where $M$ is taken to be a normal random variable with distribution $N(\mu_M, \sigma_M^2)$. As before, $W_k$ has distribution $N(\mu_W, \sigma_W^2)$. In the general case, it is not possible to write down an exact analytic expression for $\Phi$, and computer simulation must be used (§8*e*). For the special cases in which only one of $M$ or $W_k$ is random, precise treatments are possible, and details are given in §8*a*(ii), (iii).

The broken curve in figure 3*a* gives the results of a simulation for the case $R = 4$, $H = 1 + 4M\phi$, $\mu_W = 1.0$, $\sigma_W = 0.5$, $\mu_M = 1.0$, $\sigma_M = 0.1$. With these values of the standard deviations, the 'peaks' have been removed, and $\Phi$ shows a smooth dependence on $\phi$. This is already a considerable advance on the 'saw-tooth' curve; however, it is possible to go further and show that $\Phi$ can be controlled to almost a constant value over a wide range of $\phi$ values. To achieve this, a more sophisticated model of the functioning of the IIN is needed, and this is addressed in §4(*c*) below.

It is instructive to determine the IIN output that would be required if $\Phi$ were to remain exactly constant for the complete range $0 \leqslant \phi \leqslant 1$. Figure 5*a* shows the ideal total granule-cell threshold, for the case $R = 4$, $\theta_0 = 1.0$, $\sigma_W = 0.5$, $\sigma_M = 0.1$ and $\Phi = 0.2$, under the assumption that $H$ has the form $\theta_0 + MG(\phi)$. The points give values of the ideal threshold, and were calculated by numerical simulation (§8*e*). The broken line is the linear model, $H = 1 + 4\phi$, used in figure 3*a*; it can be seen that deviations from flatness in the broken curve in figure 3*a* are related to deviations in the linear threshold function (broken line) from the ideal threshold (points) in figure 5*a*. The deviation from linearity of the ideal threshold function becomes more pronounced if $\Phi$ is controlled to lower values; for example, $\Phi = 0.05$. In the next section a model IIN will be constructed which gives a much closer fit to the ideal threshold.

### (*c*) *Output with a nonlinear inhibitory interneuron*

A single IIN receives inputs from a large number $n$ of fibres (see figure 1*a*). The total input is $S = V_1 x_1 + V_2 x_2 + \ldots + V_n x_n$, where $V_i$ is the amount of transmitter released from the terminal of the $i$th input fibre, given that it is active. Suppose $V_i$ has mean $\mu_V$ and variance $\sigma_V$. (In §2 an actual distribution for a quantity such as $V$ was derived, but that much detail is not required here.) It follows that $S$ has mean $\bar{S} = n\mu_V\phi$ and variance $n\phi(1-\phi)(\mu_V^2 + \sigma_V^2) + n\phi^2\sigma_V^2$. (Cf. (39) and (40).) It is assumed that the IIN has a large diameter, like that of the Golgi cell, and consequently a relatively low input impedence; hence the effect of each quantum of transmitter secreted by the input fibre terminals will be small. If it is assumed that both $\mu_V$ and $\sigma_V$ are of order $1/n$ for $n$ large, then $\bar{S}$ is of order 1 and its standard deviation is of order $1/\sqrt{n}$, so to a good approximation $S$ can be replaced by $\bar{S}$. Thus even in the presence of variable transmitter secretion it is still reasonable to assume that the average input to the IIN is proportional to $\phi$. Consider now how the IIN responds to this input. The basic assumptions are: the activity pattern $\boldsymbol{x}$ is placed on all the input fibres simultaneously; the IIN receives an instantaneous input $\bar{S} = n\mu_V\phi$, which then decays exponentially, with time constant $1/\alpha$; while the IIN's membrane potential is above its internal threshold $h$ (assumed constant), it fires a train of impulses. (This firing rate is modelled as an inhomogeneous Poisson process, with average rate proportional to the amount by which the membrane potential exceeds $h$.) The output of the IIN is assumed to be proportional to the average number of impulses it fires.

The result of this model (see §8*c* for details) is that the output of the IIN, for an input activity level $\phi$, is proportional to $G(\phi)$, where

$$G(\phi) = \begin{cases} (\phi/\phi_0) - 1 - \ln\left(\dfrac{\phi}{\phi_0}\right), & \phi > \phi_0 \\ 0, & \phi < \phi_0. \end{cases} \qquad (17)$$

$\phi_0 = h/n\mu_V$ is the minimum activity level that will produce an output from the IIN. If (4) holds, then an expression for the total threshold $H$ has been obtained.

in figure 3*a* shows that the effect of the nonlinearity is to perform a levelling on the already-smooth output; the most important contribution to output control remains the stochastic transmitter release. (*c*) Granule-cell output for the nonlinear IIN model: different standard deviations in $W_k$ and $M$. The threshold function $H$ is the same as for (*b*). (——), $\sigma_W = 0.0$, $\sigma_M = 0.1$; (—·—), $\sigma_W = 0.5$, $\sigma_M = 0.0$; (------), $\sigma_W = 0.5$, $\sigma_M = 0.1$. Flatness could also be achieved for $\sigma_W$ smaller than 0.5 by increasing $\sigma_M$, but it is found that pattern separation suffers if $\sigma_M$ is allowed to become much larger than 0.1. Thus the most satisfactory method is to keep $\sigma_M$ at or below 0.1, and increase $\sigma_W$ until the desired level of control has been achieved. The values $\sigma_W = 0.5$, $\sigma_M = 0.1$ gives sufficient smoothing, and have been used in most of the calculations.




PHILOSOPHICAL TRANSACTIONS OF THE ROYAL SOCIETY B BIOLOGICAL SCIENCES

The effect that this inhibitory train of impulses has on the membrane potential of the granule cell remains to be seen. The simplest assumption is that the resultant hyperpolarization is proportional to the number of impulses received, i.e. to $G(\phi)$. However, this does not take into account the detailed nature of the summation process, which assigns a decreasing weight to subsequent impulses, and is particularly important in the case of inhibitory inputs in which the equilibrium potential for transmission is close to the resting membrane potential. For example, suppose the inhibition is simply due to transmitter opening channels to potassium ions. Then the total membrane potential for the granule cell, $V$, satisfies

$$I = (V - V_K)\, G_K + (V - V_A)\, G_A + C_m\, (dV/dt),$$

where subscript K refers to the potassium ions and subscript A refers to all other ions. $G_K$ and $G_A$ are conductances, $V_K$ and $V_A$ are the equilibrium potentials for potassium and other ions respectively, $C_m$ is the cell membrane capacitance and $I$ is the total current through the membrane. Under the assumption of no membrane current (i.e. $I = 0$), this has the steady-state solution

$$V - V_A = \frac{V_K - V_A}{1 + G_A/G_K}.$$

The following assumptions are now made: the arrival of the train of impulses from a single excitation of the IIN is sufficiently rapid that current loss through the granule-cell membrane can be neglected; initially, the potassium channels are closed ($G_K = 0$). The arrival of impulses opens a number of potassium channels, and the final value of $G_K$ is proportional to the total number of impulses, and thus proportional to $G(\phi)$; the total threshold is the sum of the intrinsic threshold, $\theta_0$ and the change in membrane potential due to the increase in $G_K$. It is assumed that the IIN output consists of a train of action potentials of length $cG(\phi)$, where c is a proportionality constant. Suppose that the $i$th of these releases an amount of transmitter $q_i$, where the $q_i$'s are identically distributed random variables with mean $\mu_q$ and variance $\sigma_q^2$. Then the total transmitter released is the sum of these $q_i$'s, so the average amount released is $cG(\phi)\,\mu_q$ and hence the average increase in potassium conductance will be proportional to the product $\mu_q G(\phi)$. The standard deviation of $q_{tot}$ is $\sigma_q \sqrt{(cG(\phi))}$. Provided $cG(\phi)$ is not too small, this will be small compared to the mean, and it is a good approximation to set $G_K$ proportional to $MG(\phi)$, where $M$ is proportional to $\mu_q$. The variability of $q_i$ is for a given IIN-granule cell synapse, and is thus of the type referred to as temporal variation in §2 above, whereas $\mu_q$ or $M$ varies over the whole set of granule cells, and was referred to above as spatial variation.

These assumptions lead to the following expression for the total threshold on a granule cell: $H(\phi) = \theta_0 + \theta(\phi)$, where

$$\theta(\phi) = \frac{c_1}{1 + c_2/MG(\phi)}. \qquad (18)$$

$G(\phi)$ is the output of the IIN for an input with activity level $\phi$, $M$ is a random variable and $c_1$, $c_2$ are constants.

This model of the IIN with $G(\phi)$ given by (17), together with synaptic variability, is capable of controlling the output activity on the granule cells over a wide range of input activity on the input fibres. To show this, it is first necessary to find reasonable values for the parameters $\phi_0$, $\theta_0$, $c_1$ and $c_2$ in the above expression for $H(\phi)$. This can be done by using simulation values for $H(\phi)$, such as those shown in figure 5*a* for the case $\Phi = 0.2$. It should be remarked that the simulation values shown there were calculated on the assumption that $M$ entered the threshold function linearly, as in (4). (It would not be possible to use the nonlinear form (18) without assuming a value for $c_2$.) Two comments can be made regarding this approximation. First, for $M$ not too variable and $G(\phi)$ not too large, (18) can to a good approximation be replaced by

$$\theta(\phi) \approx M \frac{c_1}{\mu_M + c_2/G(\phi)}, \qquad (19)$$

so $M$ appears essentially as a multiplicative factor. Secondly, the exact value $\Phi = 0.2$ is of no great significance, a control to $\Phi \approx 0.19$ or $\Phi \approx 0.21$ would be just as good, and this is in fact what tends to happen when the approximation (19) is used for the fitting: $\Phi$ is still controlled to an essentially constant value, but it may not be exactly the value used in the simulation of the ideal $H$.

The solid curve in figure 5*a* is the result of such a fitting, and agrees well with the simulation data in the range $0.12 < \phi < 1.0$. It is not possible to fit points below about $\phi = 0.12$ with this functional form; this is not surprising, as this corresponds to trying to control $\Phi$ to a value considerably larger than $\phi$ (i.e. an increased activity), but the role of the IIN is an inhibitory one. Also statistical fluctuations in the input $Q$ to a granule cell are large in this region. (This follows from consideration of the ratio $\sqrt{[\mathrm{var}\,(Q)]}/E(Q)$, by using (39) and (40).) Thus the fact that the analytic form does not fit for small $\phi$ is of no practical importance.

Figure 5*b* shows $\Phi$ calculated as a function of $\phi$ by using this threshold function. The 'saw-tooth' curve again shows the results of using equal fixed weights on all connections, and is only a slight improvement on the corresponding curve in figure 3*a*. The broken curve shows the simulation results when $W_k$ and $M$ are taken to be normally distributed, with means 1 and standard deviations 0.5 and 0.1, respectively. Thus $\Phi$ is maintained constant for a wide range of input activities $\phi$, by spatial and temporal variation in the amount of transmitter secreted between synapses and the non-linear behaviour of inhibitory synapses formed by the IIN.

There is some arbitrariness in the choice of the standard deviations for $W_k$ and $M$, and flatness in $\Phi$ can still be achieved by increasing one and decreasing the other. But pattern separation (see §5 below) suffers if $\sigma_M$ becomes much larger than 0.1, so this value has




PHILOSOPHICAL TRANSACTIONS OF THE ROYAL SOCIETY B BIOLOGICAL SCIENCES

been chosen for $\sigma_M$ and then $\sigma_W$ adjusted to achieve the desired control on $\Phi$. The relative importance assigned to the variability of $M$ and $W_k$ is shown in figure 5*c*: for $\sigma_W = 0$, $\sigma_M = 0.1$, the behaviour is a 'rounded saw-tooth' (solid curve), for $\sigma_W = 0.5$, $\sigma_M = 0$ it is almost flat (dot–dash curve) and close to the previous case where $\sigma_W = 0.5$, $\sigma_M = 0.1$ (broken curve).

$\Phi$ can also be controlled to other values by a suitable choice of parameters, and a number of other calculations have been performed. As already remarked, for smaller values of $\Phi$ the deviation from linearity of the ideal threshold function becomes more pronounced, but even for $\Phi = 0.05$ it is still possible to find parameter values that make the nonlinear model (18) fit reasonably well, and give an almost-level output for $\phi > 0.1$. However, the precise control of $\Phi$ becomes a rather delicate matter at very low activity levels, and a slight change in the parameters of the nonlinear INN model can have a relatively large effect.

## 5. STOCHASTIC SECRETION AND THE SEPARATION OF PATTERNS

The considerations of §4 will now be extended to pattern separation. The distinction between temporal and spatial variability in transmitter secretion now becomes important, because when patterns $\boldsymbol{x}$ and $\boldsymbol{y}$ are placed sequentially the granule-cell inputs which are active for both patterns can undergo a temporal, but not a spatial change.

### (*a*) *The effect of spatial variability in transmitter secretion*

Figure 6*a* shows $T_{xy}$ as a function of $\tau_{xy}$ for the case $\phi_x = \phi_y = 0.5$. The dotted line $T_{xy} = \tau_{xy}$ corresponds to zero improvement in pattern separation; anything below corresponds to an improvement. The solid curve is for the case where $\Phi_x$ and $\Phi_y$ are controlled to approximately 0.2 by use of the nonlinear threshold function (18) (with the usual choice of variable weights $\mu_W = \mu_M = 1.0$, $\sigma_W = 0.5$, $\sigma_M = 0.1$). The lower broken curve is for the same choice of weights, but with $\Phi_x$ and $\Phi_y$ now controlled to approximately 0.05, showing the considerable improvement in pattern separation which occurs when the output activity is lowered. The remaining (dot–dash) curve is again for $\Phi_x$ and $\Phi_y$ controlled to 0.2, but with the standard deviation of $M$ increased to 0.2, showing the reduction in pattern separation that occurs when the variability in transmission from the IIN to the granule cells is increased. Figure 6*b* shows the effect of different input activities, again with the usual choice of weights and with $\Phi_x$ and $\Phi_y$ controlled to 0.2. These again show how the separation depends on the amount by which the magnitude of the output activity $\Phi$ has been reduced below that of the input activity $\phi$.

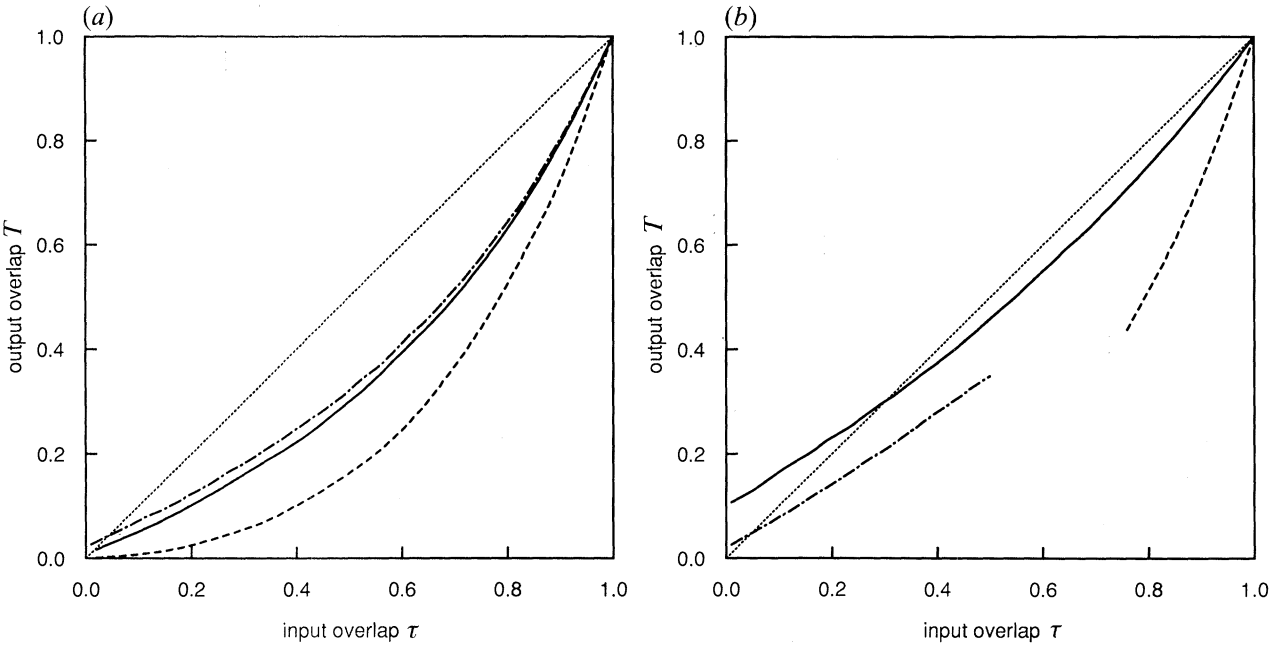


Figure 6. (*a*) Pattern separation. The output overlap $T_{xy}$ is plotted as a function of input overlap $\tau_{xy}$ for the case $R = 4$, $\phi_x = \phi_y = 0.5$, $\mu_x = \mu_y = 1.0$, $\sigma_W = 0.5$ and $\sigma_M = 0.1$ or 0.2. In each case the nonlinear threshold function (18) has been used. The line $T_{xy} = \tau_{xy}$ corresponds to no improvement in pattern separation; the region below this line represents an improvement. The most striking feature is the great improvement in pattern separation which occurs when the output activity $\Phi$ is controlled to a lower level. (——), $\Phi_x \approx \Phi_y \approx 0.2$, $\sigma_M = 0.1$; (—·—), $\Phi_x \approx \Phi_y \approx 0.2$, $\sigma_M = 0.2$; (------), $\Phi_x \approx \Phi_y \approx 0.05$, $\sigma_M = 0.1$. (*b*) Pattern separation for different input activities. In all cases $R = 4$, $\mu_x = \mu_y = 1.0$, $\sigma_W = 0.5$, $\sigma_M = 0.1$ and $\Phi_x \approx \Phi_y \approx 0.2$. (——), $\phi_x = \phi_y = 0.2$. This shows very little change in pattern separation, which is to be expected as there has been no reduction in activity. (------), $\phi_x = \phi_y = 0.8$; (—·—), $\phi_x = 0.2$, $\phi_y = 0.8$. There is separation in both cases, since there has been a reduction in activity. Note that these last two curves are only defined for a restricted range of $\tau_{xy}$ values: $\tau = 0$ corresponds to no overlap of the patterns $\boldsymbol{x}$ and $\boldsymbol{y}$, whereas $\tau = 1$ corresponds to complete overlap. These two extremes are only possible if $\phi_x = \phi_y \leqslant 0.5$; in all other cases, $\tau$ is restricted to a subrange of (0, 1).




PHILOSOPHICAL TRANSACTIONS OF THE ROYAL SOCIETY B BIOLOGICAL SCIENCES

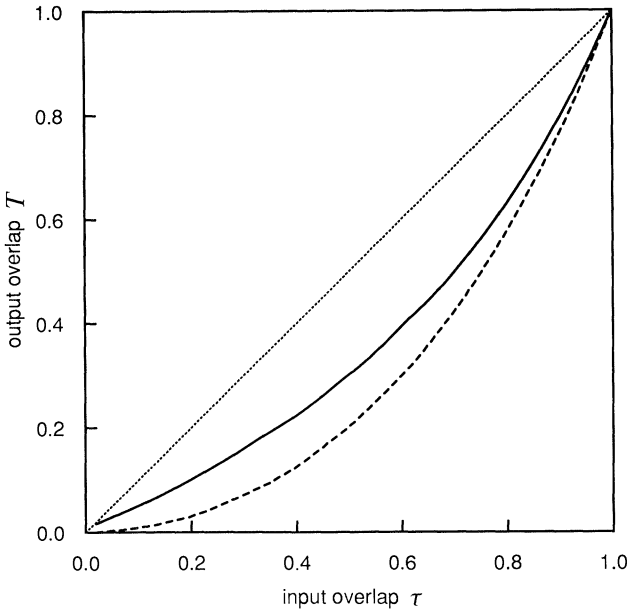


Figure 7. Pattern separation: effect of restricting the sum of weights from the input fibres to a granule cell. This implements the suggestion that the cumulative size of the terminals of a single neuron remains constant as a consequence of the way in which the terminals grow during development. The parameters are the same as for figure 6*a* with $\Phi_x \approx \Phi_y \approx 0.2$. (——), $\Sigma_{k=1}^{4} W_k$ unrestricted; (------), $\Sigma_{k=1}^{4} W_k = 4$. The graphs show that this biologically motivated restriction leads to an appreciable increase in separation.

It has been suggested that the cumulative size of the terminals of a single neuron remains constant as a consequence of the way in which the terminals grow during development (Bennett & Robinson 1989). For the granule cells this restriction means that the sum of weights, $W_1 + W_2 + .. + W_R$, is a constant $C$ which will be taken to be the same for all granule cells. This restriction is easily incorporated into the simulation programme (§8*e*). Figure 7 compares the resulting pattern separation, with (broken curve) and without (solid curve) this restriction. (The parameters are the same as for the solid curve in figure 6*a*, and $C$ is taken to be 4.) It is seen that restricting the sum of the weights considerably improves pattern separation, particularly in the region of small-to-medium overlap $\tau_{xy}$. A reason for the improvement will be discussed in the context of an analytic approximation for $\Psi_{xy}$ in §6*b* below.

### (*b*) *The effect of temporal variability in transmitter secretion*

The above calculations on pattern separation have all assumed that the entire variability of $W_k$ is a spatial one; that is, $\sigma_W = \sigma_S$, where $\sigma_S$ is the standard deviation of the spatial part of $W_k$ (see equation (16)). The effect of including temporal variability can be most clearly seen in the context of the special case where $M$ is constant. From §8*c*(iii), $\Psi_{xy}$ can be

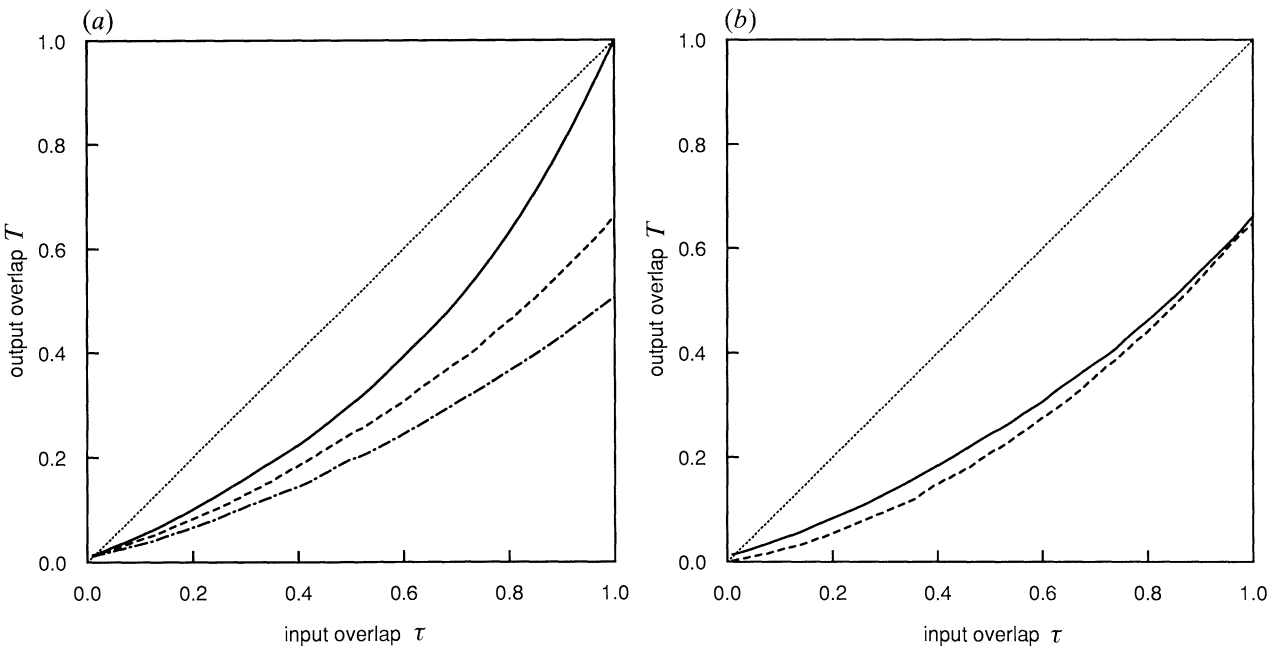


Figure 8. (*a*) Pattern separation: effect of spatial and temporal variability in the input-fibre to granule-cell weights. The total weight $W_k$, is split into two parts, $W_k = W_k^S + W_k^T$, where the spatial part $W_k^S$ has distribution $N(\mu_W, \sigma_S^2)$ and the temporal part $W_k^T$ has distribution $N(0, \sigma_T^2)$. $W_k^S$ accounts for the variability in transmitter release from one terminal to another (either on the same, or on different, granule cells); $W_k^T$ is a measure of temporal fluctuations that can occur around a mean value even for the same terminal. The output overlap $T_{xy}$ is plotted as a function of the input overlap $\tau_{xy}$ for the case $R = 4$, $\phi_x = \phi_y = 0.5$, $\mu_W = \mu_M = 1.0$, $\sigma_M = 0.1$. $\Phi_x$ and $\Phi_y$ are both controlled to approximately 0.2 by use of the nonlinear threshold function (18). (——), $\sigma_S = 0.5$, $\sigma_T = 0$; (------), $\sigma_S = \sigma_T = 0.354$; (—·—), $\sigma_S = 0$, $\sigma_T = 0.5$. Thus temporal variability enhances pattern separation, but at the expense of reliability in the network since $T$ no longer goes to 1 as $\tau$ goes to 1; this means that the same pattern presented twice will undergo a separation. (*b*) Pattern separation with both spatial and temporal variability in $W_k$ ($\sigma_S = \sigma_T = 0.354$), together with a restriction on $\Sigma_{k=1}^{4} W_k$. (——) $\Sigma_{k=1}^{4} W_k$ unrestricted; (------), $\Sigma_{k=1}^{4} W_k = 4$.

expressed in terms of bivariate normal distribution functions with correlation coefficients

$$\rho_{pqr} = r/\sqrt{(pq)}\,(\sigma_S/\sigma_W)^2, \tag{20}$$

where $p, q, r$ are summation indices. The significant feature is that $\rho_{pqr}$ decreases as the spatial variation $\sigma_S$ decreases, and so pattern separation improves. (The same trend is apparent in the analytic approximation developed in §6*b* below.) This trend is born out by simulations. Figure 8*a* shows the results for three cases: total spatial variability (solid curve), total temporal variability (dot–dash curve), and an equal mixture of both (broken curve). It is seen that the addition of temporal variability indeed enhances pattern separation, especially in the large-$\tau$ region. However, this separation is at the expense of reliability in the network since the same pattern presented twice (which corresponds to $\tau = 1$) now undergoes a separation.

The restriction that $\Sigma W_k$ be constant can be combined with the temporal variation of $W_k$, discussed in the previous section. It is clear that the restriction should apply to the spatial part of $W_k$ only, since this is the only part that the growth factor can affect. Figure 8*b* shows the separation in the case of an equal mixture of spatial and temporal variability, without (solid curve) and with (broken curve) the restriction.

## 6. ANALYTIC APPROXIMATIONS

Exact analytic expressions can be found for $\Phi$ and $\Psi_{xy}$ in a number of cases:

(i) If all the weights $W_k$ are fixed and equal, and if $M$ is also fixed, then $\Phi$ is a sum of binomial probabilities given by (25) and $\Psi_{xy}$ is a sum of multinomial probabilities given by (26).

(ii) If again all $W_k$ are fixed and equal (and for convenience taken to be unity), but $M$ is a random variable which appears linearly in the threshold function, as in (4), then the method of Torioka (1978) leads to (28) and (31).

(iii) If $M$ is fixed, and the $W_k$'s are identically distributed normal random variables, then a variation of the preceding method leads to (32) and (33) (§ 8*a* (iii)).

These special cases are of interest in their own right, and can also be used to check simulations. Once beyond them, in cases where $W_k$ and $M$ are both variable, and/or $M$ appears nonlinearly as in (18), the only accurate method available is simulation (§8*e*). However, analytic approximations are very useful for gaining insight into the detailed workings of the model, and for investigating the way in which the results depend on the parameters introduced. The following approximation uses the normal distribution, and is essentially based on the central limit theorem. For $R$ large (as in the hippocampus, see §7*b*) it is a very good approximation and can replace simulation; for $R$ small, its quantitative worth is limited, but it still gives a good qualitative explanation of many aspects of the model.

### (*a*) *An analytic approximation for the output activity of granule cells*

The output activity is given exactly by (6): $\Phi = P(Q > H)$. Application of the central limit theorem leads to the approximate expression (§8*d*)

$$\Phi \approx F_{\text{norm}}\left(\frac{E(Q)-E(H)}{\sqrt{[\text{var}\,(Q)+\text{var}\,(H)]}}\right), \tag{21}$$

where $F_{\text{norm}}$, the distribution function for the standard normal distribution, is given by (29). This is the basic equation for $\Phi$, and it remains to investigate the forms it takes in various cases.

*Case* 1. *$W_k$ and $M$ fixed*

Consider the case where the weights $W_k, k = 1, \ldots, R$, are fixed, though not necessarily equal, and $M$ is also fixed. Then (21) becomes

$$\Phi \approx F_{\text{norm}}\left(\frac{\phi \Sigma W_k - H}{\sqrt{[\phi(1-\phi)\,\Sigma W_k^2]}}\right). \tag{22}$$

It is instructive to look at $\Phi$ as a function of $H$ for fixed $\phi$. (For this exercise, take $H$ to be independent of $\phi$.) Consider first the case $W_k = 1$, $k = 1, \ldots, R$: $\Phi$ is then simply given by (11) and so is a step-function with $R$ steps. The corresponding analytic approximation, using (22), is a smooth curve and so for $R$ small it gives a drastic smoothing of the step-function. This difference is lessened if $W_k$ is allowed to take different values, as is

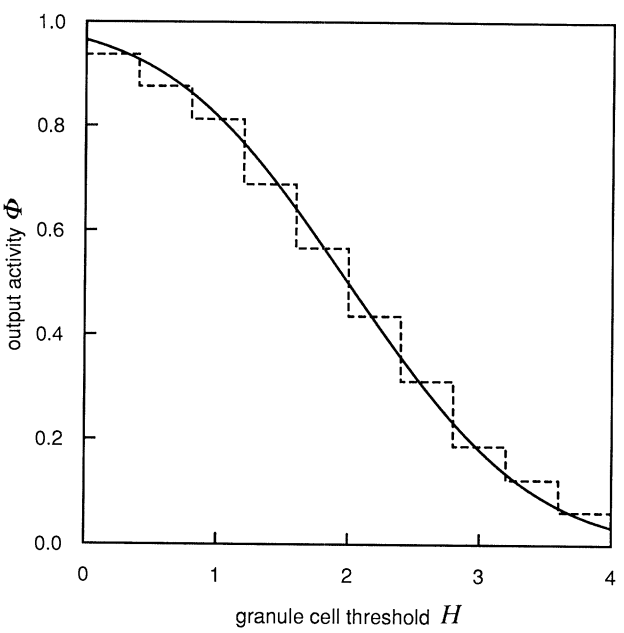


Figure 9. Comparison of the analytic approximation for $\Phi$ with exact values for the case of unequal fixed weights. The analytic approximation (22) is based on the central limit theorem, and allows $\Phi$ to be approximated by a normal distribution function. $\Phi$ is shown as a function of the granule cell threshold $H$ for the case $R = 4$, $\phi = 0.5$, $M = 1$, $W_k = 0.4, 0.8, 1.2, 1.6$. (——), analytic approximation, using (22); (------), exact, using simulation. Note that had the weights $W_k$ been equal, there would have been only four steps in the exact curve, and the approximation would have been poor. The approximation becomes more accurate as the weights become more variable, and/or $R$ becomes larger.




PHILOSOPHICAL TRANSACTIONS OF THE ROYAL SOCIETY B BIOLOGICAL SCIENCES

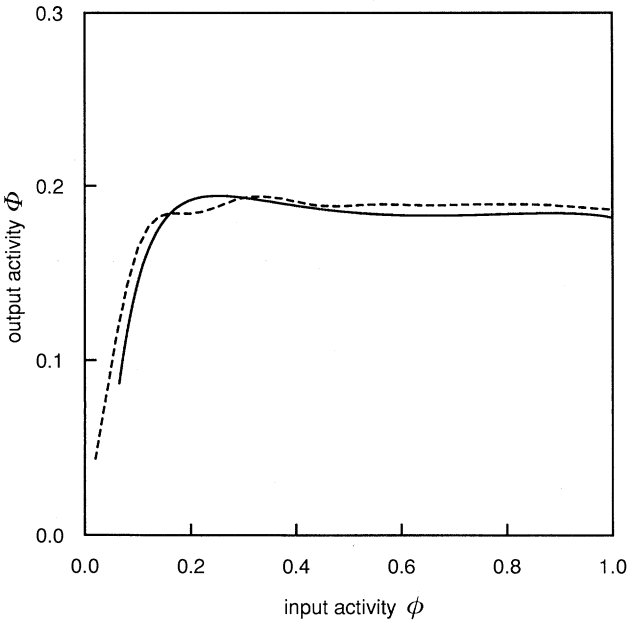


Figure 10. Comparison of the analytic approximation for $\Phi$ with exact values for the case of random weights $W_k$ and $M$. $\Phi$ is shown as a function of $\phi$ for the case $R = 4$, $\phi = 0.5$, $M$ normal, $\mu_M = 1.0$, $\sigma_M = 0.1$, $W_k$ normal, $\mu_W = 1.0$, $\sigma_W = 0.5$. (——), Analytic approximation, by using (21); (------), exact, using simulation. The agreement is excellent, showing that the stochastic variability in the weights allows this approximation to be used even for $R$ as small as 4.

shown in figure 9, where $R = 4$ and $\phi = 0.5$, but now $W_k$ takes the values 0.4, 0.8, 1.2, 1.6. The exact curve now shows many more steps (in fact 10, corresponding to the 10 distinct possible values of $Q = \Sigma W_k x_k$) and is now more closely approximated by the normal curve. Thus even for $R$ as small as 4 the analytic approximation gives a reasonably good indication of the overall behaviour of $\Phi$, as a function of $H$, if the $W_k$ take different values.

*Case 2. $W_k$ variable, $M$ fixed*

Now take the $W_k$ to be identically distributed random variables with mean $\mu_W$ and variance $\sigma_W^2$. Then the approximate $\Phi$ can be calculated from (21) using expressions for $E(Q)$ and var $(Q)$ given by (39) and (40). Calculations of $\Phi$ as a function of $H$, by using this approximation with $R = 4$, $\phi = 0.5$, $\mu_W = 1$, $\sigma_W = 0.5$, have been compared with the exact result, obtained by computer simulation, assuming $W_k$ has an $N(\mu_W, \sigma_W^2)$ distribution. The agreement is excellent over the entire range, showing that the central limit theorem, even for $R$ small, provides a very good approximation in the case where $W_k$ can take a continuous range of values.

*Case 3. $W_k$ and $M$ variable*

It is now further assumed that $M$ is a random variable with mean $\mu_M$ and variance $\sigma_M^2$. Equations (39) and (40) for $E(Q)$ and var $(Q)$ are unchanged, but expressions are needed for $E(H)$ and var $(H)$; these are given in §8*d*.

Figure 10 shows this approximation applied to the case previously considered in figure 5*b*. Agreement is excellent, with the analytic approximation smoothing out the small 'kinks' that are present in the exact case.

### (*b*) *An analytic approximation for pattern separation by granule cells*

The method of §6*a* can be extended to give an analytic approximation for $\Psi$. The result is that $\Psi_{xy}$ can be expressed as a bivariate normal distribution function; the details are in §8*d*, where the general form of the approximation is given by (42).

Calculations for the $R = 4$ case show that agreement with simulation is only moderate, with the analytic approximation giving too much separation at all overlaps $\tau_{xy}$. Agreement becomes much better for larger $R$: calculations for $R = 10$ show almost no deviation from the simulation results. Clearly, one has to be further into the asymptotic region for the bivariate normal approximation to attain comparable accuracy to the univariate one. However, even for $R = 4$ the approximation shows the correct trend, and is not too inaccurate in the small-$\tau$ region.

The bivariate-normal approximation to pattern separation provides an analytic explanation for two effects that were observed in the numerical work of §5: the increased pattern separation which occurs when the temporal variability of $W_k$ is increased, and when the sum of the $W_k$'s is fixed. In both cases the correlation coefficient $\rho$ decreases and leads to increased separation (§8*d*).

## 7. CONCLUSION: PHYSIOLOGICAL STUDIES OF THE MODEL NETWORK AND THE ROLE OF PROBABILISTIC SECRETION OF QUANTA

### (*a*) *The cerebellar granule-cell/Golgi-cell neural network*

The inhibitory interneurons associated with granule cells in the cerebellum are the Golgi cells, whereas the input axons are the mossy fibres and the output axons the parallel fibres, one per granule cell (Eccles *et al.* 1967; Llinas 1981). Golgi cells occur at low density such that a compartmentation of the space available to the Golgi cells in an idealized model of the cerebellum would consist of a hexagonal prism about 100 μm in diameter (Palkovits *et al.* 1972). Between 60 and 100 mossy fibres form excitatory synapses on a Golgi cell and these fibres are shared by the 5700 granule cells within the hexagonal prism, each of which receives an input from about four different mossy fibres (Palkovits *et al.* 1972). There is then a very large level of divergence between the mossy-fibre input and the parallel fibre output of the granule cells, of the order 10–100. Although mossy fibres terminate in a complex glomerulus, in which they make contact with the dendrites of Golgi cells and granule cells, and Golgi cell axons terminate on granule cell dendrites within the glomerulus (Chan-Palay & Palay 1971; Llinas 1981), this synaptic geometry has not been taken into consideration here. The Golgi-cell inhibition of granule-cell excitation from mossy fibres is considerable (Eccles *et al.* 1967). A single volley in the mossy fibres




PHILOSOPHICAL TRANSACTIONS OF THE ROYAL SOCIETY B BIOLOGICAL SCIENCES

gives a synaptic potential in the Golgi cell of sufficient amplitude to fire several impulses in the Golgi cell (Eccles *et al.* 1966; Eccles *et al.* 1966). These impulses give a deeper inhibition of the mossy fibre excitation of granule cells than do other forms of excitation of Golgi cells (such as that from the parallel fibres; Eccles *et al.* 1967).

The model network shown in figure 1*a* is applicable to the input stage to the cerebellum, with $n$ between 60 and 100, $N$ about 5700 and $R$ about 4. These values of $n$ and $N$ are large enough for the statistical assumptions to be valid, and so almost all the numerical examples given so far are immediately relevant to the cerebellum. In particular, figure 5*b* shows that both stochastic variability of transmitter secretion and a nonlinear Golgi cell model can give good control of the output activity level $\Phi$ and figures 6, 7 and 8 show the sorts of pattern separation that can be achieved under various conditions. The feedback from the granule cells to the Golgi cells via the parallel fibre, mentioned above, has not been included in the model network as it would only give the Golgi cell an extra constant input (proportional to $\Phi$). For the linear IIN model this would lead to an additional constant output and hence be equivalent to raising the intrinsic threshold on the granule cells; this would also be true to first order for the nonlinear model, and so the inclusion of this feedback would not alter the behaviour of the model network in any essential way.

### (*b*) *The hippocampal granule-cell/basket-cell neural network*

There are five different types of inhibitory interneurons associated with the granule cells in the fascia dentata of the hippocampus (Cajal 1911; Lorente de No 1934; Ribak & Seress 1983). Marr (1971) suggests that at least one of these types, the short axon cells in the molecular layer of the fascia dentata, provides a feedforward inhibition of the granule cells of the kind found for the pyramidal cells in the CA1 region (Algers & Nicoll 1982; Lacaille *et al.* 1987). The entorhinal cortex provides the afferent input to both inhibitory interneurons and to the granule cells via the perforant pathway (Hjorth-Simoinsen & Jeune 1972; Steward 1976). Within the rat fascia dentata there are about $10^6$ granule cells which receive about $10^5$ perforant path axons from the entorhinal cortex (Squire *et al.* 1988; McNaughton & Morris 1987). There is then a high level of divergence between the entorhinal cortex and the granule cells, of the order of 10, providing the opportunity for these cells to perform an orthogonalizing function on overlapping input patterns (McNaughton & Nadel 1989). It is not known how many perforant path axons synapse on a granule cell, but it is clearly much greater that the four mossy fibres synapsing on a granule cell in the cerebellum, as about 400 perforant axons must be stimulated to discharge a granule cell (McNaughton 1983).

Thus for the hippocampus $R$, the number of input fibres to each granule cell is at least one, if not two, orders of magnitude greater than for the cerebellum. For $R$ of the order of 100, computer simulation is very slow. Fortunately, this is precisely the region in which the analytic approximations of §6 are very accurate. (Even for $R$ as small as 4, and for random weights $W_k$ and $M$, the normal approximation to $\Phi$ was already quite accurate (see figure 10). The approximation was less good for pattern separation, but by $R = 10$ there was only a small error in the large-$\tau$ region.) Previously, computer simulation was used to find the actual shape of the granule-cell threshold $H$ as a function of $\phi$. Now the analytic approximation can be used, and from (22) an idealized threshold function is

$$H = R\phi + F^{-1}_{\text{norm}}(\Phi)\sqrt{[\phi(1-\phi)R]}, \qquad (23)$$

where $F^{-1}_{\text{norm}}$ is the inverse normal distribution function. (This equation is derived on the basis of fixed weights but will still be a good approximation provided the weights have small variances; as is shown below, satisfactory results can be achieved with $\sigma_W = 0.05$ and $\sigma_M = 0.01$.) Note that for $R$ large the second term in (23) is much smaller than the first, and so $H$ does not differ too much from having a linear dependence on $\phi$.

This threshold function is now used to find the output activity under various assumptions on the weights. For numerical illustration, the values $R = 100$ and $\Phi = 0.2$ will be used, giving $H \approx 100\phi + 8.4\sqrt{[\phi(1-\phi)]}$. For $W_k = 1$ and $M = 1$, $\Phi$ is given by (11) and figure 11*a* shows it plotted as a function of $\phi$. This is to be compared with the $R = 4$ case shown in figure 3*a*; the same saw-tooth behaviour is still present, although the frequency of the fluctuation in $\Phi$ is greater and the amplitude is less.

The output can now be smoothed by allowing stochastic variability in the weights. Figure 11*b*, calculated by using (32), shows the effect of allowing only $W_k$ to vary, with $\sigma_W = 0.05$. A similar result is obtained if $W_k$ is fixed, but $M$ is allowed to vary, with $\sigma_M = 0.01$. Note that both these standard deviations are an order of magnitude less than the values used in the $R = 4$ case. It is clear that the combination of both variabilities will be sufficient to achieve complete smoothing in the region $0.2 \lesssim \phi \lesssim 0.9$; for smaller $\phi$ there will still be some fluctuation, and for larger $\phi$ the assumed form of the threshold function $H(\phi)$ does not control $\Phi$ to 0.2. The dot–dash curve in figure 12 shows the analytic approximation (21) using these values of $\sigma_W$ and $\sigma_M$.

The threshold function (23) was obtained by the purely mathematical device of requiring the analytic approximation (22) to give a constant output $\Phi$. This can be related to the nonlinear model of an inhibitory interneuron developed in §4*c*, by using the fitting procedure described in the legend to figure 5. The resulting output is the solid curve in figure 12, showing that reasonably good control can be achieved with the nonlinear IIN model in the region $0.15 \lesssim \phi \lesssim 0.9$. The broken curve in figure 12 is obtained using $H = 100\phi + 3.36$, which is a linear fit to (23). Pattern separation can also be calculated for this model, using the analytic approximation (42) with the nonlinear threshold function. Significant separation is found, comparable to the best separation in figure 6*a*.

Overall, it can be concluded for the large-$R$ case that stochastic variability of transmitter secretion is still




PHILOSOPHICAL TRANSACTIONS OF THE ROYAL SOCIETY B BIOLOGICAL SCIENCES

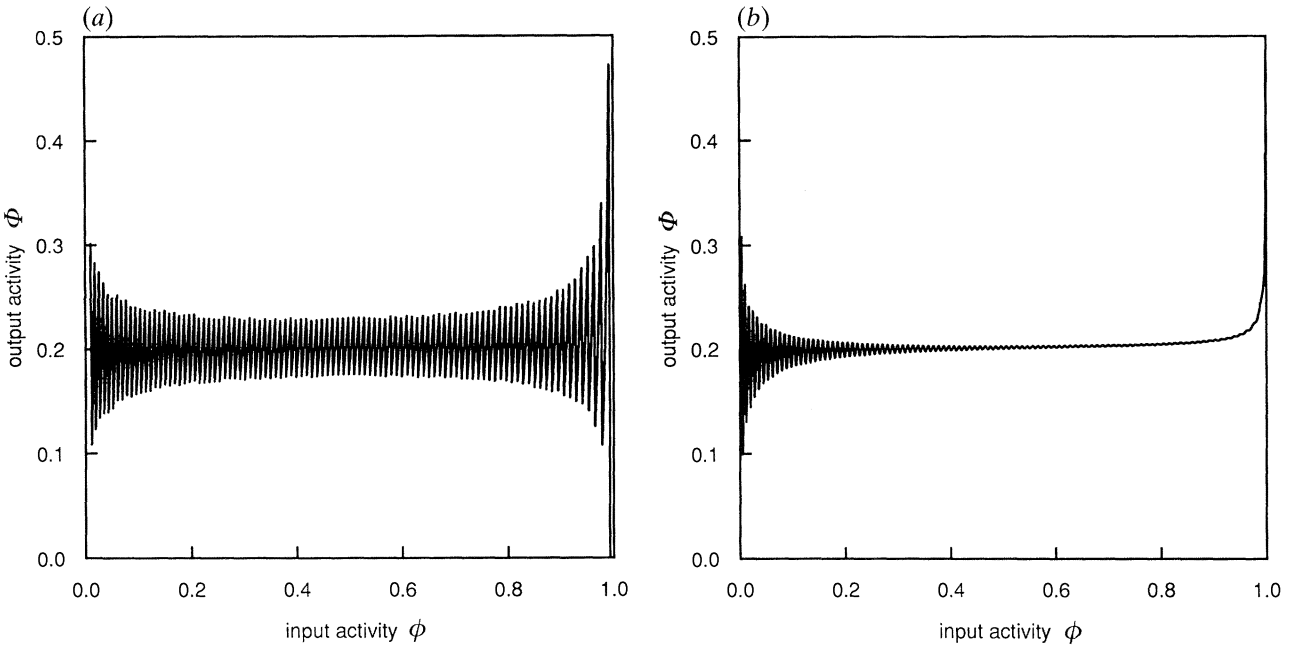


Figure 11. Granule-cell output for a network with a large number of inputs to each granule cell. $R = 100$ and the granule-cell threshold function $H$ is given by (23). This could have application to the input of the hippocampus. (*a*) Fixed synaptic weights: $W_k = 1$ and $M = 1$. The fluctuations in output are related to the 'saw-tooth' behaviour found in the $R = 4$ case (figure 3*a*), but have greater frequency and smaller amplitude. The calculation uses (11). (*b*) Variable weights on the inputs to the granule cells: $\mu_W = 1$, $\sigma_W = 0.05$, $M = 1$. Considerable smoothing has now been achieved in all except the small-$\phi$ region. Note that the standard deviation $\sigma_W = 0.05$ is an order of magnitude less than that required to smooth the $R = 4$ case, indicating that less stochastic variability is needed in the hippocampus. The calculation uses (32). A similar smoothing can be achieved by taking $W_k$ fixed and $M$ variable.

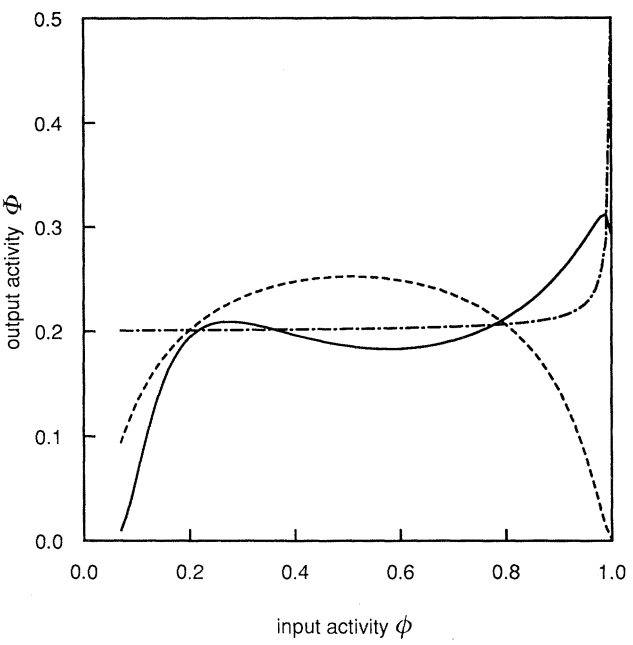


Figure 12. Granule-cell output for $R = 100$ and various choices of the threshold function $H$. In each case the weights are variable, with means 1 and $\sigma_W = 0.05$, $\sigma_M = 0.01$. The calculations use the analytic approximation (21). (——), Nonlinear model (18). The actual function used is $H = 12.5 + 415/(1.0 + 59.5/(20\phi - 1.0 - \ln(20\phi)))$; (------), linear model: $H = 100\phi + 3.36$; (—·—), idealized model (23). The idealized model gives the flattest output, but this is artificial since it was constructed purely for that purpose. More significant is the fact that the nonlinear model, which does have a biological basis, can also give satisfactory control.

important, although the magnitude of this variability can be considerably less than for the small-$R$ case. Also, the nonlinear model of the IIN can give satisfactory threshold control on the granule cells, although the deviation from linearity is now not so pronounced.

### (*c*) *Experimental testing of the model networks and the role of probabilistic secretion of quanta*

The proposed role of activity regulation by the granule cell network described above can be tested experimentally for both the cerebellum and the hippocampus as follows. Stimulating electrodes placed on the input to an impaled granule cell (either the mossy fibres of the cerebellum or the pyriform pathway axons of the hippocampus) allow varying numbers of input axons to be excited, depending on the strength of the stimulation (a relative estimate of the numbers of these axons could be ascertained by recording the field potential near them). The firing or not of the granule cell at each stimulus level (proportional to $\phi$) would then be noted and the procedure repeated for at least 20 granule cells receiving this input from these axons; averaging over the results for the 20 or more granule cells at each stimulus strength should then give an estimate of the activity regulation of the network; that is, the value of $\Phi$ for each $\phi$. Blocking inhibitory transmission from the interneurons to the granule cells and repeating the above procedure would test the role of the inhibitory interneuron (IIN). It might also be possible to test for the role of stochastic temporal variability at synapses in activity regulation by




PHILOSOPHICAL TRANSACTIONS OF THE ROYAL SOCIETY B BIOLOGICAL SCIENCES

repeating the above procedures for determining $\phi$ and $\Phi$ after blocking autoinhibition at the granule-cell synapses. It has been shown that blocking autoinhibition at excitatory synapses, which is often mediated by adenosine (see, for example, Dunwiddie & Hoffer 1980; Bennett & Robinson 1990; Bennett *et al.* 1990), can greatly increase the stochastic temporal variability. These experiments may be most appropriately carried out on *in vitro* slices of the hippocampus or the cerebellum, cut in such a way as to include the lamellae organization of the axon inputs to the granule cells in the slice.

The proposed role of pattern separation by the granule-cell network can be tested in an analogous way to that for activity regulation. In this case, however, at least three stimulating electrodes are required on separate components of the axon input to the granule cells. One of these electrodes is always stimulated in conjunction with either of the two, and the axons it excites constitute the overlapping component of the patterns. Changes in the strengths of the stimulations from these electrodes will modify $\tau_{xy}$ and recording of the firing or not over a large number ($>20$) of granule cells will allow estimates of $T_{xy}$, in an analogous way to the estimate of $\Phi$. The contribution of the inhibitory interneuron and of stochastic variability to pattern separation may also be tested with appropriate blocking drugs.

### (*d*) *Output control and memory storage*

One very important reason for controlling granule-cell activity to a low level is related to the possible storage of the resulting output patterns in later stages of the cerebellum or the hippocampus. It has been shown for a variety of theoretical memory-storage models that sparse encoding of the information to be stored considerably increases both the number of patterns that can be stored and the reliability of recall (Amit *et al.* 1987; Palm 1988; Amari 1989). The present work emphasizes the vital role played by the stochastic secretion of transmitter in achieving the necessary sparseness.

## 8. APPENDIX

### (*a*) *Analytic expressions for granule-cell output and pattern separation in various cases*

(i) $W_k = 1$, $M =$ *constant*

For the special case where all $W_k = 1$, and $M$ is a constant, simple analytic expressions can be found for $\Phi$ and $\Psi$ (Torioka 1978). Let $A$ be the number of active inputs to the granule cell. Then, from (6),

$$\Phi = \sum_{k=1}^{R} P(Q > H \,|\, A = k)\, P(A = k), \tag{24}$$

where the $k = 0$ term is omitted, since it is assumed that the granule cell does not fire spontaneously. As each input has the same probability $\phi$ of being active, this leads to

$$\Phi = \sum_{k>H}^{R} b(k; R, \phi), \tag{25}$$

where $b(k; R, \phi)$ is the binomial probability function

$$b(k; R, \phi) \equiv \binom{R}{k} \phi^k (1-\phi)^{R-k}.$$

Consider now patterns $\boldsymbol{x}$ and $\boldsymbol{y}$, and let $A_x$, $A_y$, $A_{xy}$ be the number of inputs active for $\boldsymbol{x}$, for $\boldsymbol{y}$, and for both $\boldsymbol{x}$ and $\boldsymbol{y}$, respectively. Then, from (10),

$$\begin{aligned}\Psi_{xy} &= \sum_{p=1}^{R}\sum_{q=1}^{R}\sum_{r=\max(0,\,p+q-R)}^{\min(p,\,q)} \\ &\quad \times P(Q_x > H_x, Q_y > H_y \,|\, A_x = p, A_y = q, A_{xy} = r) \\ &\quad \times P(A_x = p, A_y = q, A_{xy} = r) \\ &= \sum_{p>H_x}^{R}\sum_{q>H_y}^{R} W_{pq},\end{aligned} \tag{26}$$

where

$$W_{pq} = \sum_{r=\max(0,\,p+q-R)}^{\min(p,\,q)} W_{pqr} \tag{27}$$

and $W_{pqr}$ is the multinomial distribution:

$$\begin{aligned}W_{pqr} &= \frac{R!}{(p-r)!\,(q-r)!\,r!\,(R-p-q+r)!} \\ &\quad \times (\phi_x - \psi_{xy})^{p-r}\,(\phi_y - \psi_{xy})^{q-r} \\ &\quad \times (\psi_{xy})^{r}\,(1-\phi_x-\phi_y+\psi_{xy})^{R-p-q+r}.\end{aligned}$$

(ii) *Analytic expressions for the case* $W_k = 1$, $M$ *random*

For the special case where all $W_k = 1$, and $M$ enters the threshold equation linearly, as in equation (4), analytic expressions can be found for $\Phi$ and $T$, analogous to those of Torioka (1978, 1979). Equation (24) still holds with $P(A = k)$ binomial as before, but now

$$P(Q > H \,|\, A = k) = P[M^* < \alpha_k(\phi)],$$

where (3) and (4) have been used for $H$, $M^* = (M-\mu_M)/\sigma_M$ and $\alpha_k(\phi) = [k-\theta_0-\mu_M\,\theta(\phi)]/[\sigma_M\,\theta(\phi)]$. Thus

$$\Phi = \sum_{k=1}^{R} F_{M^*}[\alpha_k(\phi)]\, b(k; R, \phi), \tag{28}$$

where $F_{M^*}(x)$ is the distribution function for $M^*$. Under the usual assumptions, $M^*$ will have the standard normal distribution $N(0, 1)$, and so $F_{M^*}$ is $F_{\text{norm}}$, where

$$F_{\text{norm}}(x) = \frac{1}{\sqrt{(2\pi)}} \int_{-\infty}^{x} \mathrm{e}^{-t^2/2}\,\mathrm{d}t \tag{29}$$

is the standard normal distribution function. From (26),

$$\Psi_{xy} = \sum_{p=1}^{R}\sum_{q=1}^{R} P(p > H_x, q > H_y)\, W_{pq}, \tag{30}$$

where $W_{pq}$ is given by (27). Thus

$$\Psi_{xy} = \sum_{p=1}^{R}\sum_{q=1}^{R} P\{M^* < \alpha_p(\phi_x), M^* < \alpha_q(\phi_y)\}\, W_{pq},$$
$$= \sum_{p=1}^{R}\sum_{q=1}^{R} \min\{F_{M^*}[\alpha_p(\phi_x)], F_{M^*}[\alpha_q(\phi_y)]\}\, W_{pq}. \quad (31)$$

(iii) *Analytic expressions for the case $W_k$ random, $M$ constant*

Consider now the case where $M$ is constant, and for convenience set $M = 1$. If it is further assumed that the weights $W_k$ are identically distributed normal random variables with distribution $N(\mu_W, \sigma_W^2)$, then the following modification of the method of Appendix $a$(ii) gives exact analytic expressions for $\Phi$ and $\Psi_{xy}$. $\Phi$ is still given by (24), but in evaluating $P(Q > H | A = k)$ use is made of the fact that $Q$ is the sum of identically distributed normal random variables, and so is normal itself with distribution $N(k\mu_W, k\sigma_W^2)$. Thus

$$\Phi = \sum_{k=1}^{R} F_{\text{norm}}[\beta_k(\phi)]\, b(k; R, \phi), \quad (32)$$

where $\beta_k(\phi) = (k\mu_W - \theta_0 - \theta(\phi))/(\sigma_W\sqrt{k})$.

$\Psi_{xy}$ is given by (26), where $(Q_x, Q_y)$ is now bivariate normal, with correlation coefficient

$$\rho_{pqr} = \frac{\text{cov}\,(Q_x, Q_y | A_{xy} = r)}{\sqrt{[\text{var}\,(Q_x | A_x = p)\,\text{var}\,(Q_y | A_y = q)]}}.$$

Now $Q_x = \Sigma_{k=1}^{R} W_k x_k$ and $Q_y = \Sigma_{k=1}^{R} W'_k y_k$, where each $W_k, W'_k$ consists of both a spatial and a temporal part, as in (15). This splitting makes no difference to the variances, and $\text{var}\,(Q_x | A_x = p) = p\sigma_W^2$, $\text{var}\,(Q_y | A_y = q) = q\sigma_W^2$, but because the temporal parts corresponding to $\boldsymbol{x}$ and $\boldsymbol{y}$ are independent, $\text{cov}\,(W_k, W'_k) = \sigma_S^2$, where $\sigma_S$ is the standard deviation of the spatial part of $W_k$ and hence $\text{cov}\,(Q_x, Q_y | A_{xy} = r) = r\sigma_S^2$. Thus $\rho_{pqr} = [r/\sqrt{(pq)}]\,(\sigma_S/\sigma_W)^2$ and

$$\Psi_{xy} = \sum_{p=1}^{R}\sum_{q=1}^{R}\sum_{r=\max(0,\,p+q-R)}^{\min(p,\,q)} \times L[-\beta_p(\phi_x), -\beta_q(\phi_y), \rho_{pqr}]\, W_{pqr}, \quad (33)$$

where

$$L(h, k, \rho) = \int_h^\infty \mathrm{d}x \int_k^\infty [2\pi\sqrt{(1-\rho^2)}]^{-1} \times \exp\left[-\frac{1}{2}\left(\frac{x^2 - 2\rho xy + y^2}{1-\rho^2}\right)\right]\mathrm{d}y \quad (34)$$

is the bivariate normal probability function (Abramowitz & Stegun 1965).

Even if the $W_k$ are not normally distributed, the above formulae will still be approximately true, the accuracy becoming better as $R$ increases.

### (*b*) *The relation between spatial and temporal variability of synapses and probabilistic firing of neurons*

In the formalism used in this paper, the effect that the firing of a neuron has on other neurons is contained entirely in the weights of the synaptic connections between them. As discussed in §2, these weights contain both a temporal part describing variations in successive firings at a given terminal and a spatial part describing variations from terminal to terminal. The total weight is thus time-dependent.

A number of neural network theories use an alternative formalism in which the connecting weights include only the spatial variability (and hence are time-independent), while the temporal variability is accounted for by making the firing of the neuron depend on its total input in a probabilistic way (Little 1974; Peretto 1984). Specifically, the probability of a neuron firing is taken to be

$$\bar{\mathscr{P}} = \frac{1}{1 + \exp[-\beta(\bar{Q} - \theta_0)]}, \quad (35)$$

where $\bar{Q}$ is the total input calculated by using time-independent weights, $\theta_0$ is the intrinsic threshold and $\beta$ is a parameter. This form was originally chosen to exploit an analogy between model neural networks and a statistical-mechanical system of interacting spins (Little 1974); more generally, this choice ensures that the equilibrium state of the system is the Boltzmann distribution and allows techniques developed for the analysis of spin-glass systems to be applied to neural networks (Peretto 1984; Amit, Gutfreund & Sompolinsky 1985). The form (35) has also been justified on biological grounds (Shaw & Vaseudevan 1974; Burnod & Korn 1989).

The purpose of this section is to show the relation of the present approach to the probabilistic firing formalism. Consider a single neuron with $R$ inputs, weights $W_k$, $k = 1, 2, \ldots, R$ and intrinsic threshold $\theta_0$. Suppose a specific firing pattern $\boldsymbol{x} = (x_1, x_2, \ldots, x_R)$, where $x_i = 0, 1$, is placed on these inputs, so that the total input to the neuron is $Q = \Sigma_k W_k x_k$. In the present formalism, $W_k$ can be written as the sum of a spatial part $W_k^S$ and a temporal part $W_k^T$ (see (15)), and corresponding to this division, $Q = Q^S + Q^T$, where $Q^S = \Sigma_k W_k^S x_k$ and $Q^T = \Sigma_k W_k^T x_k$. Suppose the same pattern $x$ is placed repeatedly on the inputs to this neuron. Then $Q^S$ is a constant, but $Q^T$ is a random variable which, under the assumptions of §2, has an $N(0, r\sigma_T^2)$ distribution, where $r$ is the number of active inputs under pattern $x$. The probability that this neuron fires is thus

$$\mathscr{P} = P(Q > \theta_0) = P\left(\frac{Q - E(Q)}{\sqrt{[\text{var}\,(Q)]}} > \frac{\theta_0 - E(Q)}{\sqrt{[\text{var}\,(Q)]}}\right).$$

Since $E(Q) = Q^S$, $\text{var}\,(Q) = r\sigma_T^2$ and $[Q - E(Q)]/\sqrt{[\text{var}\,(Q)]}$ has an $N(0, 1)$ distribution, this becomes

$$\mathscr{P} = F_{\text{norm}}[(Q^S - \theta_0)/(\sigma_T\sqrt{r})], \quad (36)$$

where $F_{\text{norm}}$ is given by (29).

This is now to be related to $\bar{\mathscr{P}}$, as given by (35). It is clear that $\bar{Q} = \Sigma_{k=1}^{R} W_k^S x_k \equiv Q^S$, since in the probabilistic-firing model only the spatial variability is placed in the synaptic weights. Expression (35) is then a very good approximation to (36) if the choice $\beta = [4/\sqrt{(2\pi)}]\,(1/\sigma_T\sqrt{r})$ is made. (This gives $\mathscr{P}$ and $\bar{\mathscr{P}}$ the

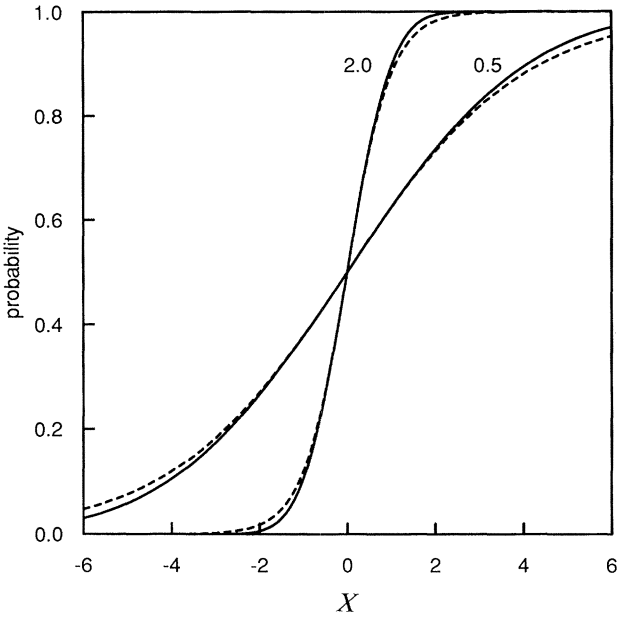


Figure 13. Comparison of two expressions for the probability that a neuron fires when its potential is $x$ above threshold: (——), probability $= F_{\text{norm}}(\sqrt{(2\pi)}\,\beta x/4)$ (equation (36)); (------), probability $= 1/(1+\exp(-\beta x))$ (equation (35)). The two cases are $\beta = 2.0$ and $\beta = 0.5$.

same slope at $Q^S = \theta_0$.) Figure 13 shows the agreement between the functions $\mathscr{P} = F_{\text{norm}}(\sqrt{(2\pi)}\,\beta x/4)$ (solid lines) and $\bar{\mathscr{P}} = 1/[1+\exp(-\beta)]$ (broken lines) for the cases $\beta = 2.0$ and $\beta = 0.5$. Note that $\beta$ is inversely proportional to the standard deviation of the temporal variation in $W_k$, which is in accord with its statistical-mechanical interpretation as an inverse temperature.

### (*c*) *Nonlinear model for the inhibitory interneuron*

This section provides the details of the derivation of (17) for the output of the nonlinear model of the inhibitory interneuron described in §4*c*. Under the assumptions stated there, provided $\bar{S} > h$, the IIN fires in the time-interval $0 \leqslant t \leqslant T$, where $T$ is given by $\bar{S}\,\mathrm{e}^{-\alpha T} = h$ and its firing rate is governed by the parameter $\beta(t) = \bar{S}\,\mathrm{e}^{-\alpha t} - h$. Hence the total number of impulses fired is

$$\int_0^T \beta(t)\,\mathrm{d}t = \begin{cases} (1/\alpha)\,(\bar{S}-h) - (h/\alpha)\ln\left(\dfrac{\bar{S}}{h}\right), & \bar{S} > h \\ 0, & \bar{S} < h. \end{cases}$$

Using $\bar{S} = n\mu_V\,\phi$, this can be written as

$$\int_0^T \beta(t)\,\mathrm{d}t = \begin{cases} (h/\alpha)\,[(\phi/\phi_0) - 1 - \ln(\phi/\phi_0)], & \phi > \phi_0 \\ 0, & \phi < \phi_0, \end{cases}$$

where $\phi_0 = h/n\mu_V$. Thus the output of the IIN, for an input activity level $\phi$, is proportional to $G(\phi)$ as given by (17).

### (*d*) *Analytic approximations for granule-cell output and pattern separation*

To obtain an analytic approximation for the granule-cell output activity $\Phi$, write (6) as

$$\Phi = P\left(\frac{Z-E(Z)}{\sqrt{(\mathrm{var}\,(Z))}} > \frac{-E(Z)}{\sqrt{(\mathrm{var}\,(Z))}}\right), \tag{37}$$

where $Z \equiv Q-H$, $E(Z)$ is the expected value of $Z$ and $\mathrm{var}\,(Z)$ is its variance, and then approximate it by $\Phi \approx F_{\text{norm}}(E(Z)/\sqrt{[\mathrm{var}\,(Z)]})$, where $F_{\text{norm}}(x)$, the distribution function for the standard normal distribution, is given by (29). Putting $Z = Q-H$ then gives

$$\Phi \approx F_{\text{norm}}\left(\frac{E(Q)-E(H)}{\sqrt{[\mathrm{var}\,(Q)+\mathrm{var}\,(H)]}}\right). \tag{38}$$

If $W_k$ has a $N(\mu_W, \sigma_W^2)$ distribution, then the mean and variance of $Q$ are

$$E(Q) = \phi R\mu_W, \tag{39}$$

$$\mathrm{var}\,(Q) = \phi(1-\phi)\,R(\mu_W^2+\sigma_W^2) + \phi^2 R\sigma_W^2. \tag{40}$$

If $M$ has a $N(\mu_M, \sigma_M^2)$ distribution and $H$ has the form $H = \theta_0 + MG(\phi)$, where $G(\phi)$ is independent of $M$, then $E(H) = \theta_0 + \mu_M\,G(\phi)$ and $\mathrm{var}\,(H) = \sigma_M^2[G(\phi)]^2$. If $H$ has the more complicated dependence on $M$ given by (18) then a further approximation is needed. If $f(M)$ is a differentiable function of the random variable $M$ and $\sigma_M \ll \mu_M$, then $E[f(M)] \approx f(\mu_M)$ and $\mathrm{var}\,[f(M)] \approx [f'(\mu_M)]^2\,\sigma_M^2$ (Cramer 1946). Taking $f(M) = Mc_1/[M + c_2/G(\phi)]$ leads to

$$E(H) \approx \theta_0 + \frac{\mu_M\,c_1}{\mu_M + c_2/G(\phi)},$$

$$\mathrm{var}\,(H) \approx \frac{(c_1\,c_2/G(\phi))^2}{[\mu_M + c_2/G(\phi)]^4}\,\sigma_M^2.$$

It turns out that in practice these corrections due to variable $M$ are small, and the above approximations are entirely adequate.

The above method can be extended to give an analytic approximation for $\Psi$. One starts by writing (10) as

$$\Psi_{xy} = P\left(\frac{Z_x-E(Z_x)}{\sqrt{[\mathrm{var}\,(Z_x)]}} > \frac{E(Z_x)}{\sqrt{[\mathrm{var}\,(Z_x)]}},\ \frac{Z_y-E(Z_y)}{\sqrt{[\mathrm{var}\,(Z_y)]}} > \frac{E(Z_y)}{\sqrt{[\mathrm{var}\,(Z_y)]}}\right), \tag{41}$$

where $Z_x \equiv Q_x - H_x$, $Z_y \equiv Q_y - H_y$. This is now approximated by a bivariate normal distribution:

$$\Psi_{xy} \approx L\left(\frac{E(H_x)-E(Q_x)}{\sqrt{[\mathrm{var}\,(H_x)+\mathrm{var}\,(Q_x)]}}, \frac{E(H_y)-E(Q_y)}{\sqrt{[\mathrm{var}\,(H_y)+\mathrm{var}\,(Q_y)]}}, \rho\right), \tag{42}$$

where

$$\rho = \frac{\mathrm{cov}\,(Q_x, Q_y) + \mathrm{cov}\,(H_x, H_y)}{\sqrt{[\mathrm{var}\,(H_x)+\mathrm{var}\,(Q_x)]\,[\mathrm{var}\,(H_y)+\mathrm{var}\,(Q_y)]}}. \tag{43}$$

The distribution function $L(h, k, \rho)$ is given explicitly by (34). These expressions can be evaluated for various cases but here we given only the case of main interest, which is $W_k$ and $M$ both variable. The means and variances can be found from (39) and (40), and the covariance is calculated to be

$$\text{cov}\,(Q_x, Q_y) = (\psi_{xy} - \phi_x \phi_y)\, R(\mu_W^2 + \sigma_S^2) + \phi_x \phi_y R \sigma_S^2.$$

Note that in the covariance the distinction between spatial and temporal variation in the synaptic weights becomes important (see the discussion surrounding (15) and (16)): it is $\sigma_S$ and not $\sigma_W$ that appears in the expression for the covariance, since the temporal variations in the $\boldsymbol{x}$- and $\boldsymbol{y}$-inputs are uncorrelated.

If $H$ has the simpler form $H = \theta_0 + MG(\phi)$, then $E(H) = \theta_0 + \mu_M G(\phi)$, $\text{var}\,(H) = [G(\phi)]^2 \sigma_M^2$ and $\text{cov}\,(H_x, H_y) = G(\phi_x)\, G(\phi_y)\, \sigma_M^2$. For the more general form (18),

$$E(H) \approx \theta_0 + \frac{\mu_M c_1}{\mu_M + c_2/G(\phi)},$$

$$\text{var}\,(H) \approx \frac{[c_1 c_2/G(\phi)]^2}{[\mu_M + c_2/G(\phi)]^4} \sigma_M^2,$$

$$\text{cov}\,(H_x, H_y) \approx \frac{[c_1 c_2/G(\phi_x)]\,[c_1 c_2/G(\phi_y)]}{[\mu_M + c_2/G(\phi_x)]^2\,[\mu_M + c_2/G(\phi_y)]^2} \sigma_M^2.$$

The last result is derived by using $\text{cov}\,(f(M), g(M)) \approx f'(\mu_M)\, g'(\mu_M)\, \sigma_M^2$. Substitution of these expressions in (42) and (43) gives the final expression for $\Psi_{xy}$.

Equation (42) provides an analytic explanation for two effects which were observed in the numerical work in §5. The first is the increased pattern separation that occurs when the temporal variability of $W_k$ is increased. That this will happen is clear from the above formulae: as $\sigma_S$ is decreased, with $\sigma_W$ kept constant, the variances of $Q_x$ and $Q_y$ remain unchanged but the covariance will decrease. Thus the correlation coefficient $\rho$, given by (43), will decrease and hence pattern separation will increase. The second effect is the increased pattern separation that occurs when the sum of weights on the input fibres to a granule cell is restricted. If $\sum_{k=1}^{R} W_k =$ constant, then the variance and covariance of $Q$ must be replaced by $\text{var}\,(Q_z) = \phi_z(1-\phi_z)\, R(\mu_W^2 + \sigma_W^2) + \phi_z^2 R \sigma_T^2$ and $\text{cov}\,(Q_x, Q_y) = (\psi_{xy} - \phi_x \phi_y)\, R(\mu_W^2 + \sigma_S^2)$. In this case both the covariance and the variance are reduced, but the overall effect is to cause a reduction in $\rho$ and hence enhanced pattern-separation. For example, for the case $R = 4$, $\mu_W = 1$, $\sigma_W = \sigma_S = 0.5$, $\sigma_M = 0$, $\phi_x = \phi_y = 0.5$, $\rho$ changes from $(10\psi_{xy} - 2)/3$ to $4\psi_{xy} - 1$ upon imposition of the restriction $\Sigma W_k = 4$. This causes a reduction in $\rho$ over the entire range of $\psi_{xy} (0 \leqslant \psi_{xy} \leqslant 0.5)$, with the largest reduction being for small $\psi_{xy}$, in accordance with figure 7.

### (*e*) *Simulation methods*

There are two aspects to the simulation of the network of figure 1: the first is the generation of random input patterns $\boldsymbol{x}$ and the second is the incorporation of the variable weights $W_k$ and $M$. To find the output activity $\Phi$ for an input pattern of activity $\phi$, one generates random numbers $S_k$ uniformly distributed on (0, 1), and sets $x_k = 1$ if $S_k$ is in the subinterval $(0, \phi)$ and $x_k = 0$ otherwise. The $x_k$'s are then random variables with $P(x_k = 1) = \phi$. A complete pattern would consist of $x_1, x_2, \ldots, x_n$, since there are $n$ input fibres. However, a single granule cell has only $R$ inputs and it is therefore only necessary to generate $R$ numbers $x_1, x_2, \ldots, x_R$ for each simulation trial. $R$ random variables $W_k$ are then chosen from the distribution $N(\mu_W, \sigma_W^2)$ and the sum $Q = \sum_{k=1}^{R} W_k x_k$ evaluated to give the total input $Q$ to the granule cell. The granule cell threshold is now set, using $M$ taken from $N(\mu_M, \sigma_M^2)$ in $H = \theta_0 + MG(\phi)$ (or in the more accurate expression (18)), and the output is then 1 if $Q > H$ and 0 otherwise. This completes one simulation trial. In the next trial, a new set of $x_k$'s is generated, and also new $W_k$'s and $M$ are chosen from the normal distributions. This corresponds to sampling from a different (randomly chosen) granule cell: the new set $x_1, x_2, \ldots, x_R$ can be thought of as either a different part of the same complete pattern $x_1, x_2, \ldots, x_n$ or, equivalently, part of a new pattern with the same activity $\phi$; the new choice of weights corresponds to taking a different granule cell. In this way a network with an arbitrary number of input fibres and granule cells can be investigated by doing simulations on a simple network with $R$ inputs and one output. The output activity $\Phi$ is then found by repeating the above procedure $N_S$ times and computing the average number of times the output is 1. Typically, $N_S$ was taken to be 10000; this still left some statistical fluctuations, and the data were smoothed before being graphed.

For pattern separation, one must consider two input patterns $\boldsymbol{x}$ and $\boldsymbol{y}$; these are placed sequentially and independently on the inputs but, for the purposes of collecting statistics on the output, both members of a pair must be treated together. There are now four events to be considered: a given input fibre may be active under (i) $\boldsymbol{x}$ only; (ii) $\boldsymbol{y}$ only; (iii) both; (iv) neither. The corresponding probabilities are (i) $\phi_x - \psi_{xy}$, (ii) $\phi_y - \psi_{xy}$, (iii) $\psi_{xy}$, (iv) $1 - \phi_x - \phi_y + \psi_{xy}$. The interval (0, 1) is divided into four subintervals with lengths equal to these probabilities, and random numbers $S_k, k = 1, 2, \ldots, R$, uniformly distributed on (0, 1), are again generated. $x_k$ and $y_k$ are then assigned values according to the position of $S_k$, e.g. if $S_k$ falls in the first subinterval $\phi_x - \psi_{xy}$ then $x_k = 1$ and $y_k = 0$, corresponding to the $k$th input being active under pattern $\boldsymbol{x}$ but inactive under $\boldsymbol{y}$. Again $R$ random variables $W_k$ are chosen from the distribution $N(\mu_W, \sigma_W^2)$ and the sums $Q_x = \sum_{k=1}^{R} W_k x_k$, $Q_y = \sum_{k=1}^{R} W_k y_k$ calculated. Note that the division of $W_k$ into spatial and temporal parts (see (15)) is now important: in calculating the contributions to $Q_x$ and $Q_y$ the same spatial weight $W_k^S$ (but a different temporal weight $W_k^T$) must be used in the region $\psi_{xy}$, where both $x_k = 1$ and $y_k = 1$. The same applies to $M$ since, as discussed in §4*c*, it takes into account a spatial variability. The thresholds $H_x$ and $H_y$ are now set, and the firing of the granule cell under each pattern noted. Again, a large number of repetitions are performed, and these can be thought of as sampling from randomly chosen granule




PHILOSOPHICAL TRANSACTIONS OF THE ROYAL SOCIETY B BIOLOGICAL SCIENCES

cells, either under the same input patterns on the whole set of $n$ input fibres, or under different input patterns with the same $\phi_x$, $\phi_y$ and $\psi_{xy}$. $\Phi_x$ and $\Phi_y$ are calculated as the fraction of times the output is 1 under $\boldsymbol{x}$ and $\boldsymbol{y}$, respectively, and $\Psi_{xy}$ as the fraction of times it is 1 under both pairs of input patterns.

The restriction $\Sigma_{k=1}^{R} W_k = C$ (see §5) was implemented by taking $R$ random numbers $Q_k$ from an $N(0, \sigma_Q^2)$ distribution, and forming $W_k = Q_k + C/R - (1/R)\Sigma_{j=1}^{R} Q_j$. $W_k$ then has mean $C/R$ and standard deviation $\sigma_W = \sigma_Q\sqrt{(1-1/R)}$.

## REFERENCES


Abramowitz, M. & Stegun, I. A. 1965 *Handbook of mathematical functions*, ch. 26.3.3. New York: Dover.

Albus, J. 1971 A theory of cerebellar function. *Math. Biosci.* **10**, 25–61.

Algers, B. E. & Nicoll, R. A. 1982 Feed-forward dendritic inhibition in the rat hippocampal pyramidal cells studied in vitro. *J. Physiol., Lond.* **328**, 105–123.

Amari, S. 1989 Characteristics of sparsely encoded associative memory. *Neural Networks* **2**, 451–457.

Amit, D., Gutfreund, H. & Sompolinsky, H. 1985 Spin-glass models of neural networks. *Phys. Rev.* A **32**, 1007–1018.

Amit, D., Gutfreund, H. & Sompolinsky, H. 1987 Information storage in neural networks with low levels of activity. *Phys. Rev.* A **35**, 2293–2303.

Bennett, M. R., Fisher, C., Florin, T., Quine, M. & Robinson, J. 1977 The effect of calcium ions and temperature on the binomial parameters that control acetycholine release by a nerve impulse at amphibian neuromuscular synapses. *J. Physiol., Lond.* **271**, 641–672.

Bennett, M. R., Karunanithi, S. & Lavidis, N. A. 1991 Probabilistic secretion of quanta from nerve terminals in toad (*Bufo marinus*) muscle modulated by adenosine. *J. Physiol., Lond.* **239**, 329–358.

Bennett, M. R. & Robinson, J. 1989 Growth and elimination of nerve terminals at synaptic sites during polyneuronal innervation of muscle cells: a trophic hypothesis. *Proc. R. Soc. Lond.* B **235**, 299–320.

Bennett, M. R. & Robinson, J. 1990 Probabilistic secretion of quanta from nerve terminals at synaptic sites on muscle cells: non-uniformity, autoinhibition and the binomial hypothesis. *Proc. R. Soc. Lond.* B **239**, 329–358.

Burnod, Y. & Korn, H. 1989 Consequences of stochastic release of neurotransmitters for network computation in the central nervous system. *Proc. natn. Acad. Sci. U.S.A.* **86**, 352–356.

Cajal, S. R. 1911 *Histologie du système nerveux*, tome II. Madrid: C.S.I.C.

Chan-Palay, V. & Palay, S. L. 1971 The synapse en marron between Golgi II neurons and mossy fibres in the rat's cerebellar cortex. *Z. Anat. EntwGesch.* **133**, 274–287.

Cramer, H. 1946 *Mathematical methods of statistics*, pp. 354, 366. Princeton University Press.

Dunwiddie, T. V. & Hoffer, B. J. 1980 Adenine nucleotides and synaptic transmission in vitro rat hippocampus. *Br. J. Pharmac.* **69**, 59–68.

Eccles, J. C., Ito, M. & Szentagothai, J. 1967 *The cerebellum as a neuronal machine*. Heidelberg: Springer-Verlag.

Eccles, J. C., Llinas, R. & Sasaki, K. 1966 The mossy fibre-granule cell relay of the cerebellum and its inhibitory control by Golgi cells. *Expl Brain Res.* **1**, 82–101.

Eccles, J. C., Sasaki, K. & Strata, P. 1966 Interpretation of the potential fields generated in the cerebellar cortex by a mossy fibre volley. *Expl Brain Res.* **3**, 58–80.

Eccles, J. C., Sasaki, K. & Strata, P. 1967 A comparison of the inhibitory actions of Golgi cells and of basket cells. *Expl Brain Res.* **3**, 81–94.

Hjorth-Simoinsen, A. & Jeune, B. 1972 Origin and termination of the hippocampal perforant path in the rat studied by silver impregnation. *J. comp. Neurol.* **144**, 215–232.

Katz, B. 1969 The release of neural transmitter substances. In *The Sherrington lectures*, vol. x. Liverpool University Press.

Korn, H. & Faber, D. S. 1987 Regulation and significance of probabilistic release mechanisms at central synapses. In *Synaptic functions* (ed. G. Edelman, E. Gall & M. Cowan), pp. 57–108. New York: Wiley.

Lacaille, J. C., Mueller, A. L., Kunkel, D. D. & Schwartzkroun, P. A. 1987 Local circuit interactions between oriens/alveus interneurons and CA1 pyramidal cells in hippocampal slices: electrophysiology and morphology. *J. Neurosci.* **7**, 1979–1993.

Little, W. A. 1974 The existence of persistent states in the brain. *Mathl Biosci.* **19**, 101–120.

Little, W. A. & Shaw, G. L. 1975 A statistical theory of short and long term memory. *Behav. Biol.* **14**, 115–133.

Llinas, R. 1981 Electrophysiology of the cerebellar networks. In *Handbook of physiology* (ed. J. M. Brookhart & V. B. Mountcastle). Section I, The nervous system. Vol. II, *Motor control*, part 2, pp. 831–876. Bethesda: American Physiological Society.

Lorente de Nó, R. 1933 Studies on the structure of the cerebral cortex. I. The area entorhinalis. *J. Psychol. Neurol., Lpz.* **45**, 381–438.

Lorente de Nó, R. 1934 Studies on the structure of the cerebral cortex. II. Continuation of the study of the ammonic system. *J. Psychol. Neurol., Lpz.* **46**, 113–177.

Marr, D. 1969 A theory of cerebellar cortex. *J. Physiol., Lond.* **202**, 437–470.

Marr, D. 1970 A theory for cerebral neocortex. *Proc. R. Soc. Lond.* B **176**, 161–234.

Marr, D. 1971 Simple memory: a theory for archicortex. *Phil. Trans. R. Soc. Lond.* B **262**, 23–81.

McLachlan, E. M. & Martin, A. R. 1981 Non-linear summation of end-plate potentials in the frog and mouse. *J. Physiol., Lond.* **311**, 307–324.

McNaughton, B. L. 1983 Activity dependent modulation of hippocampal synaptic efficacy: some implications for memory processes. In *Neurobiology of the hippocampus* (ed. W. Seifert). New York: Academic Press.

McNaughton, B. L. & Morris, R. G. M. 1987 Hippocampal synaptic enhancement and information storage within a distributed memory system. *Trends Neurosci.* **10**, 408–425.

McNaughton, B. L. & Nadel, L. 1989 Hebb–Marr networks and the neurobiological representation of action in space. In *Neuroscience and connectionist theory* (ed. M. A. Gluck & D. E. Rumelhart). New Jersey: Lawrence Erlbaum Associates.

Palkovits, M., Magyar, P. & Szentagothai, J. 1972 Quantitative histological analysis of the cerebellar cortex in the cat. IV. Mossy fibre–Purkinje cell numerical transfer. *Brain Res.* **45**, 15–29.

Palm, G. 1988 Local synaptic rules with maximal information storage capacity. In *Neural and synergetic computers* (ed. H. Haken), pp. 100–110. Berlin: Springer-Verlag.

Peretto, P. 1984 Collective properties of neural networks: a statistical physics approach. *Biol. Cybern.* **50**, 51–62.

Redman, S. 1990 Quantal analysis of synaptic potentials in neurons of the central nervous system. *Physiol. Rev.* **70**, 165–198.

Redman, S. J. & Walmsley, B. 1982 Amplitude fluctuations in synaptic potentials evoked in cat spiral motoneurones at identified group 1A synapses. *J. Physiol., Lond.* **343**, 135–145.

Ribak, C. E. & Seress, L. 1983 Five types of basket cell in the hippocampal dentate gyrus; a combined Golgi and electron microscope study. *J. Neurocytol.* **12**, 577–597.

Robinson, J. 1976 Estimation of parameters for a model of transmitter release at synapses. *Biometrics* **32**, 61–68.

Shaw, G. L. & Vasudevan, R. 1974 Persistent states of neural networks and the random nature of synaptic transmission. *Math. Biosci.* **21**, 207–218.

Steward, O. 1976 Topographic organization of the projections from the entorhinal area to the hippocampal formation of the rat. *J. comp. Neurol.* **167**, 285–314.

Squire, L. R., Shimamura, A. P. & Amaral, D. G. 1988 Memory and the hippocampus. In *Neural models of plasticity* (ed. J. H. Byrne & W. O. Berry), pp. 208–239. San Diego: Academic Press.

Torioka, T. 1978 Pattern separability and the effect of the number of connections in a random neural net with inhibitory connections. *Biol. Cybern.* **31**, 27–35.

Torioka, T. 1979 Pattern separability in a random neural net with inhibitory connections. *Biol. Cybern.* **34**, 53–62.

Torioka, T. & Ikeda, N. 1988 Pattern separating functioning of two-layered random nerve nets with feedforward inhibitory connections. *IEEE Trans. Syst. Man Cyb.* **18**, 358–366.

Willis, J. B. 1975 A review of some theoretical models of the brain. *Prog. Neurobiol.* **5**, 245–270.

Willis, J. B. 1986 The modelling of neural circuitry. *Prog. Neurobiol.* **26**, 93–118.

*Received 21 June 1990; revised 24 September 1990; accepted 1 February 1991*



PHILOSOPHICAL TRANSACTIONS OF THE ROYAL SOCIETY B BIOLOGICAL SCIENCES